Biometals (2021) 34:529–556
https://doi.org/10.1007/s10534-021-00293-1

Structural elucidation, theoretical investigation, biological screening and molecular docking studies of metal(II) complexes of NN donor ligand derived from 4-(2-aminopyridin-3-methylene)aminobenzoic acid

Ramaiah Konakanchi · Geetha Swarupa Pamidimalla · Jyothi Prashanth · Togati Naveen · Laxma Reddy Kotha

Received: 19 November 2020 / Accepted: 12 February 2021 / Published online: 2 March 2021

Abstract Complexes of 4-(((2-aminopyridin-3-yl)methylene)amino)benzoic acid ligand with cobalt(II) (**1**), nickel(II) (**2**), copper(II) (**3**), zinc(II) (**4**) and palladium(II) (**5**) are synthesized and characterized by using different spectroscopic methods like, UV–Visible, infrared, ^{1}H, ^{13}C NMR, molar conductance, ESR and elemental analysis. Quantum chemical computations were made using DFT (density functional theory), B3LYP functional and 6-31+ +G(d,p)/SDD basis set in order to determine optimized structure parameters, frontier molecular orbital parameters and NLO properties. Based on DFT and experimental evidence, the complexes ensured that the octahedral geometry have been proposed for complexes **1**, **2** and **4,** square planar for complexes **3** and **5**. All the complexes showed only residual molar conductance values and hence they were considered as non-electrolytes in DMF. In addition, the anti-proliferative activity of the compounds was evaluated against different human cancer cell lines (IMR-32, MCF-7, COLO205, A549, HeLa and HEK 293) and cisplatin is used as a reference drug. Compounds **1** and **4** showed remarkable cytotoxicity in five cancer cell lines tested except MCF-7. Also, the compounds were examined for their in vitro antimicrobial and scavenging activities. The molecular docking results are well corroborated with the experimental anticancer activity results.

Keywords 4-(((2-Aminopyridin-3-yl)methylene)amino)benzoic acid · DFT calculations · Molecular docking · Antimicrobial · Anti-proliferative activity

Supplementary Information The online version contains supplementary material available at https://doi.org/10.1007/s10534-021-00293-1.

R. Konakanchi
Chemistry Division, H&S Department, Malla Reddy Engineering College for Women (Autonomous Institution), Hyderabad 500100, India

R. Konakanchi · L. R. Kotha (✉)
Department of Chemistry, National Institute of Technology, Warangal 506004, India
e-mail: laxmareddychem12@gmail.com

G. S. Pamidimalla
Chemistry Division, H&S Department, Malla Reddy College of Engineering for Women, Hyderabad 500014, India

J. Prashanth
Department of Physics, Kakatiya University, Warangal 506009, India

T. Naveen
Applied Chemistry Department, S. V. National Institute of Technology, Surat 395007, India

Introduction

Cancer, one of the most staggering and death causing diseases in the world involves abnormal cell proliferation in the body (Mahmoud et al. 2018; Thirunavukkarasu et al. 2018; Devi et al. 2018a, b). On one hand cisplatin and its derivatives, on the other hand, a large number of metal complexes are introduced in the treatment of a variety of cancers. In 2015 about 90.5 million individuals were accounted for to have cancer (Srividya et al. 2019). Along these lines, there have been instances of various sorts of tumors which reach up to an incredible number of 14.1 million every year and the sickness has nearly asserted about 8.8 million lives (15.7%) till date (Global et al. 2016). In this regard, metal complexes having sulphur and nitrogen atoms in the core moiety of ligands are one of the growing interest fields of coordination chemistry (Mohammadtabar et al. 2016), owing to activity binding and cleaving the DNA under physiological conditions (Muralisankar et al. 2016). For the past few decades, metal complexes like platinum and copper complexes occupy an eminent position in cancer diagnosis and treatment (Wernyj et al. 2004; Ramadan et al. 2018). Some of the metal complexes having anticancer activity were shown in Fig. 1 (Muralisankar et al. 2016; Kelland et al. 2007). However, it was observed that there are several drawbacks regarding the usage of complexes like dose limiting efficiency, limited clinical usage to several tumors, a wide range of side effects (Wernyj et al. 2004). Hence, the chemists make serious efforts to design, develop, synthesis new, safe drug-like molecules with high selectivity, maximum efficacy and minimum toxicity. One among them Schiff base metal complexes have a broad spectrum of pharmacological properties (Abdel-Rahman et al. 2015, 2016; Abdel Aziz et al. 2017a, b). These complexes also remarkable biological activities like antioxidant, antitumor antimicrobial, anti-inflammatory, antimalarial (Khedr et al. 2012; Mesbah et al. 2018; Miri et al. 2013; Mumtaz et al. 2016; El-Boraey and El-Salamony 2019).

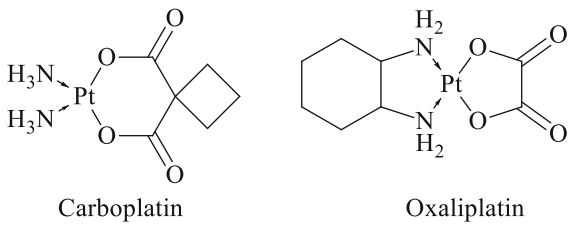

Carboplatin Oxaliplatin

Fig. 1 Some representative examples for the metal complexes having the anticancer activity

In view of the aforementioned biological importance of the metal complexes and Schiff bases, herewith we report the novel metal complexes of Pd(II), Zn(II), Cu(II), Ni(II) and Co(II) with Schiff base in a single molecular framework and their potential in vitro anticancer, antioxidant, antimicrobial activities and in silico studies (DFT and molecular docking).

Results and discussion

Synthesis

The new ligand (L) was prepared by treating 4-aminobenzoic acid with 2-aminonicotinaldehyde under stirring conditions (Scheme 1). The metal(II) complexes (**1–5**) were synthesized by mixing the different metal chlorides with ligand in methanol. The resulting mixtures were refluxed for 4 h at 70 °C (Scheme 2). The complexes are stable at room temperature and are non-hygroscopic. Analytical data of the compounds are presented in Table 1. All the complexes are soluble in DMSO and dimethylformamide but insoluble in common organic solvents. The authenticities of the synthesized compounds were ascertained using various spectroscopic methods and elemental analysis.

Spectroscopy

The rationale positions of the selected characteristic IR bands unambiguously unveiled the formation of ligand 4-(((2-aminopyridin-3-yl)methylene)amino)benzoic acid and its metal complexes. The important absorption frequencies are presented in Table 2. The ligand showed the strong band at 1629 cm^{-1} due to ν(C=N), on the other hand, this band is lowered by 20–30 cm^{-1} in the complexes pointing to the fact that the nitrogen of this group is involved in binding with the metal ion (Ebrahimi et al. 2014; Abu Al-Nasr and Ramadan 2013; Ramadan et al. 2014; Abdel Aziz et al. 2017a, b). The amine group nitrogen of the ligand showed the band at 3420 cm^{-1} due to ν(NH_2) has been found lower frequencies by (3401–3371 cm^{-1}) in the complexes,

Scheme 1 Synthetic route of ligand (**L**)

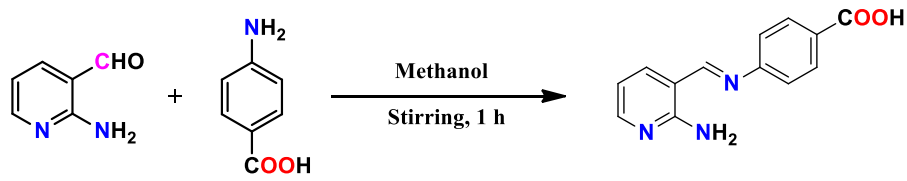

Scheme 2 Synthetic route of the mental(II) complexes

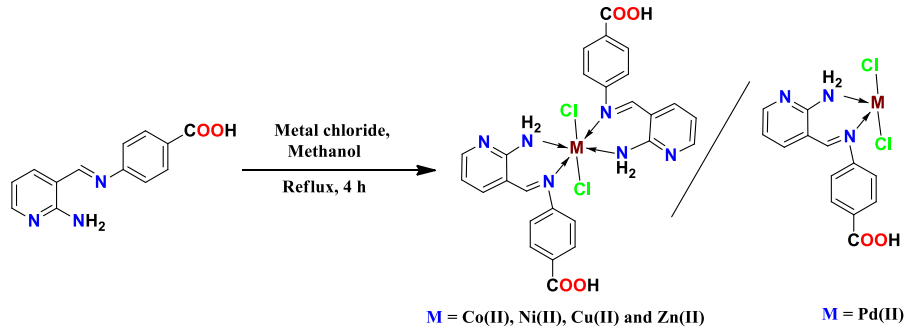

Table 1 Analytical and physical parameters for the ligand (**L**) and its metal complexes (**1–5**)

Molecular formula	Formula weight	Colour (yield %)	Melting point (°C)	Elemental analyses: found (calculated)				
				C	N	H	M	Molar cond
$C_{26}H_{22}Cl_2CoN_6O_4$ (**1**)	612.33	Brown (71)	350–352	50.93 (51.00)	13.66 (13.72)	3.65 (3.62)	9.69 (9.62)	12
$C_{26}H_{22}Cl_2N_6NiO_4$ (**2**)	612.09	Light green (79)	310–312	50.97 (51.02)	13.67 (13.73)	3.58 (3.62)	9.52 (9.59)	16
$C_{26}H_{22}Cl_2CuN_6O_4$ (**3**)	616.94	Green (84)	328–330	50.58 (50.62)	13.59 (13.62)	3.55 (3.59)	10.25 (10.30)	19
$C_{26}H_{22}Cl_2N_6O_4Zn$ (**4**)	618.78	Light yellow (75)	378–380	50.41 (50.47)	13.54 (13.58)	3.55 (3.58)	10.50 (10.57)	15
$C_{13}H_{11}Cl_2N_3O_2Pd$ (**5**)	418.57	Orange (88)	336–338	37.37 (37.30)	10.09 (10.04)	2.59 (2.65)	25.31 (25.42)	11
$C_{13}H_{11}N_3O_2$ (**L**)	241.25	Yellow (95)	270–272	64.65 (64.72)	17.48 (17.42)	4.56 (4.60)	–	–

this kind of shift suggested that amine nitrogen is bonded to the metal (Burns 1968; Jyothi et al. 2015). The carboxylic acid (C=O) and $(C=N)_{py}$ stretching frequencies of the ligand occurring at 1701 and 1567 cm^{-1}. These bands do not undergo any perceptible shifts in the metal complexes suggesting that there are no interactions between oxygen and nitrogen of these groups. The aforementioned results proved that the ligand coordinating with metal ions through the amine nitrogen atom and the azomethine nitrogen. In complexes (**1–5**) the peaks observed in the range of 478–520 cm^{-1} and 275–321 cm^{-1} corresponds to υ(M–N) and υ(M–Cl), respectively. The conductance measurements of the metal complexes (**1–5**) in DMF

Table 2 Infrared absorption frequencies (cm^{-1}) of ligand (**L**) and its metal complexes (**1–5**)

Compound	υ(N–H)	υ(C=N) azomethine	υ(C=N)(py)	υ(C=O) carboxylic acid	υ(M–Cl)	υ(M–N)
1	3371	1604	1564	1699	321	493
2	3389	1663	1569	1704	275	520
3	3390	1590	1562	1703	284	501
4	3384	1592	1571	1697	315	481
5	3401	1608	1570	1705	292	478
L	3420	1629	1567	1701	–	–

solution were made at 10^{-3} mol dm^{-3} concentrations. All the complexes showed only residual molar conductance values (11–19 Ω^{-1} cm^2 mol^{-1}) and hence they may be considered as non-electrolytes (Saif et al. 2011; Firdaus et al. 2009). This implies that both the two chloride anions associated with these complexes are present inside the coordination sphere. Thus these compounds may be formulated as $[ML_2Cl_2]$. The results are given in Table 1. The UV–Visible spectra of the ligand exhibited the bands at 30,390 cm^{-1} and 33,245 cm^{-1} corresponding to n → π* and π → π* transitions, respectively. The electronic spectra of Co(II) complex (**1**) exhibits three bands around 9000 cm^{-1} ($^4T_{1g}(F) \rightarrow {}^4T_{2g}(F)$ (ϑ_1)), 18,500 cm^{-1} ($^4T_{1g}(F) \rightarrow {}^4A_{2g}(F)$ (ϑ_2)) and 20,400 cm^{-1} attributable to $^4T_{1g}(F) \rightarrow {}^4T_{1g}(P)$, respectively, characteristic of octahedral geometry (Shukla et al. 2008; Chandra 2004). The octahedral geometry is also more supports the ϑ_2/ϑ_1 value, which fall in the range (2.02) observed for the octahedral complex (Devi et al. 2018a, b). The Racah inter electronic repulsion parameter (B) value for the Co(II) complex was found to be 756 cm^{-1} which is lower than the free ion value (B^1 = 971 cm^{-1}) indicates a good overlap of the orbitals involved (Konakanchi et al. 2018a, b). Further, the nephelauxetic effect parameter ($\beta = B/B^1$) value (0.78) is less than one suggesting that M–L bonds are covalent in character. The results are given in Table 3. The Ni(II) complex exhibits three peaks in the region of 9800, 15,900 and 25,800 cm^{-1}. These peaks have been attributed, respectively to the transitions $^3A_{2g}(F) \rightarrow {}^3T_{2g}(F)$, $^3A_{2g}(F) \rightarrow {}^3T_{1g}(F)$ and $^3A_{2g}(F) \rightarrow {}^3T_{1g}(P)$ of octahedral geometry (Nigam et al. 2000; Saleh 2005; Saif et al. 2012). And also the value ϑ_2/ϑ_1 (1.61) further supports the octahedral geometry. The values of B (820 cm^{-1}) and β (0.80) observed for Ni(II) complex indicate that the orbital overlap and M–L bonds are covalent in character (Devi et al. 2018a, b). The Cu(II) complex reveals a peak at 18,351 cm^{-1} and a shoulder at 13,825 cm^{-1}, respectively as is usually expected for square planar geometry (Raman et al. 2004). Zn(II) complex shows no bands in the visible region as is expected for d^{10} system and also showed the peak around 28,500 cm^{-1} due to charge transfer. Octahedral geometry has been proposed based on the empirical formulae (Ganesan et al. 2019; Devi et al. 2012), Pd(II) complex show three peaks at 18,700 ($^1A_{1g} \rightarrow {}^1A_{2g}$), 21,500 ($^1A_{1g} \rightarrow {}^1B_{1g}$) and 24,850 cm^{-1} ($^1A_{1g} \rightarrow {}^1E_g$) these transitions characteristic of square-planar geometry (Goggin et al. 1972). Further the band at 28,000 cm^{-1} is due to the charge transfer. Further, the ϑ_2/ϑ_1 value (1.14) also supports the square planar geometry (Gajendragad and Aggarwala 1975). The Co(II), Ni(II) complexes observed magnetic moment (μ_{eff}) values are 4.95, 3.22 BM, respectively suggests

Table 3 Electronic spectral data, ligand field parameters and magnetic data of the complexes (**1–5**)

Complexes	Frequencies (cm^{-1})	Assignments	μ_{eff} (BM)	ϑ_2 / ϑ_1	10 DQ (cm^{-1})	B (cm^{-1})	β	Geometry
1	9000	$^4T_{1g}(F) \rightarrow {}^4T_{2g}(F)$ (υ_1)						
	18,500	$^4T_{1g}(F) \rightarrow {}^4A_{2g}(F)$ (υ_2)	4.95	2.02	9250	756	0.78	Octahedral
	20,400	$^4T_{1g}(F) \rightarrow {}^4T_{1g}(P)$ (υ_3)						
2	9800	$^3A_{2g}(F) \rightarrow {}^3T_{2g}(F)$ (υ_1)						
	15,900	$^3A_{2g}(F) \rightarrow {}^3T_{1g}(F)$ (υ_2)	3.22	1.61	9800	820	0.80	Octahedral
	25,800	$^3A_{2g}(F) \rightarrow {}^3T_{1g}(P)$ (υ_3)						
3	13,825	$^2B_{1g} \rightarrow {}^2E_g$	1.90	–	–	–	–	Distorted octahedral
	18,351	$^2B_{1g} \rightarrow {}^2B_{2g}$						
4	–	–	Diamagnetic	–	–	–		Octahedral
5	18,700	$^1A_{1g} \rightarrow {}^1A_{2g}$	Diamagnetic	1.14	–	–	–	Square planar
	21,500	$^1A_{1g} \rightarrow {}^1B_{1g}$						
	24,855	$^1A_{1g} \rightarrow {}^1E_g$						
	28,000	Charge transfer						

the octahedral arrangement (Omar and Mohamed 2005; Patil and Kulkami 1984; Ramadan 2012; Mohamed et al. 2001; Cotton et al. 1999; Kavitha , 2012). From the literature, the square planar copper(II) complexes, μ_{eff} values are observed in the range of 1.82–1.86 B.M. (Sabastiyan and Venkappayya 1990). In the present investigation, the μ_{eff} value is 1.83 B.M. which indicates a square planar arrangement. The Zn(II) and Pd(II) complexes are diamagnetic. The results are given in Table 3. In the ^{1}H NMR spectra of the ligand, the carboxylic acid attached O–H proton showed the signals at 12.93 ppm. In the complexes, this O–H proton observed the signals around 12.82–12.07 ppm. In the ligand, the azomethine CH proton and NH_2 attached pyridine ring was observed at 8.72 ppm and 7.38 ppm, respectively. In the spectra of complexes, the azomethine CH and NH_2 protons appeared in the range of 8.74–8.61 ppm (CH=N) and 7.33–7.28 ppm (NH_2), respectively. ^{13}C NMR spectra of the ligand showed the chemical shift values at 167.49, 163.88 and 158.44 ppm indicate the carboxylic acid (C=O), (C=N) and (C–NH_2) groups, respectively. The aromatic carbons were observed in the range of 158.44–112.34 ppm. The ^{1}H and ^{13}C NMR spectra of the ligand and its metal complexes were shown in Figs. 2, 3 and 4, respectively.

DFT computations

Required calculations were made using the Gaussian 09/DFT program package (Frisch et al. 2010). Beck's three parameter hybrid exchange functional B3 (Becke 1993) in conjunction with Lee-Yang-Parr (LYP) correlation functional (Lee et al. 1988) using enlarged basis set 6-311+ +G(d,p) /SDD was employed for the purpose. These basic functionals are more accurate and reduce the computational rate and include few relativistic effects in the calculations (Bergner et al. 1993; Kaupp et al. 1991; Dolg et al. 1993). The optimized molecular geometry for the ligand and its metal complexes (**1**–**5**) were shown in Fig. 5. The results of bond angles, bond lengths and dihedral angles were presented in Tables 4 and 5. On the optimization of geometry, the observed global minimum energy of the compounds were observed at − 816.95688 Hartree (ligand), − 2698.19907 Hartree (**1**), − 2723.30339 Hartree (**2**), − 2749.76705 Hartree (**3**), − 2779.56640 Hartree (**4**) and − 1865.00019 Hartree (**5**), respectively.

Molecular electronic properties i.e. electron affinity (A), ionization potential (I), chemical potential (μ), global hardness (η) and global electrophilicity power (ω) of ligand and its metal complexes obtained from frontier molecular orbital energies comprising of highest occupied molecular orbital (HOMO) and lowest unoccupied molecular orbital (LUMO) using the following expressions (Gece 2008; Fukui 1982; Koopmans 1933; Parr et al. 1999).

$$\begin{aligned} I &= -E_{HOMO};\ A = -E_{LUMO}; \\ &= (-E_{HOMO} + E_{LUMO})/2;\ \mu \\ &= (E_{HOMO} + E_{LUMO})/2;\ \text{and}\ \omega = \mu^2/2 \end{aligned}$$

HOMO and LUMO are known as frontier molecular orbitals. They are important in quantum chemistry, as they determine the molecular reactivity of conjugated systems (Choi and Kertez 1997) and the ability of a molecule to absorb electromagnetic radiation. HOMO plays the role of an electron donor, whereas LUMO act as an electron acceptor (Gece 2008; Fukui 1982). The results are presented in Table 6 and illustrated in Fig. 6. The molecules under consideration, the FMO energy gap was found to be **L > 3 > 2 > 5 > 1 > 4**. Generally, molecules with a small frontier orbital gap are readily polarizable and normally exhibit high chemical reactivity and low kinetic stability (Sinha et al. 2011; Lewis et al. 1994; Kosar and Albayrak 2011). The FMO gap of metal complexes (**1**–**5**) are small compared to the ligand, hence the metal complexes are more polarizable than the ligand (Table 6). As the chemical potential (μ) for the compounds being investigated are negative (Table 6) it is stable.

Non-linear optical (NLO) behavior

DFT has been widely used as a powerful method to examine the NLO materials (Prasad and Wiliams 1991). To understand NLO behavior of the ligand and its metal complexes, computation of the total molecular dipole moment (μ_t) and its components, total molecular polarizability (α_t) and its components, anisotropy of polarizability ($\Delta\alpha$), and first order static hyperpolarizability (β_t) was attempted according to Buckingham's definition (Buckingham 1967) using density functional theory based on finite field approach. Generally, polarizabilities (α_t) and first order hyperpolarizabilities (β_t) were estimated to the

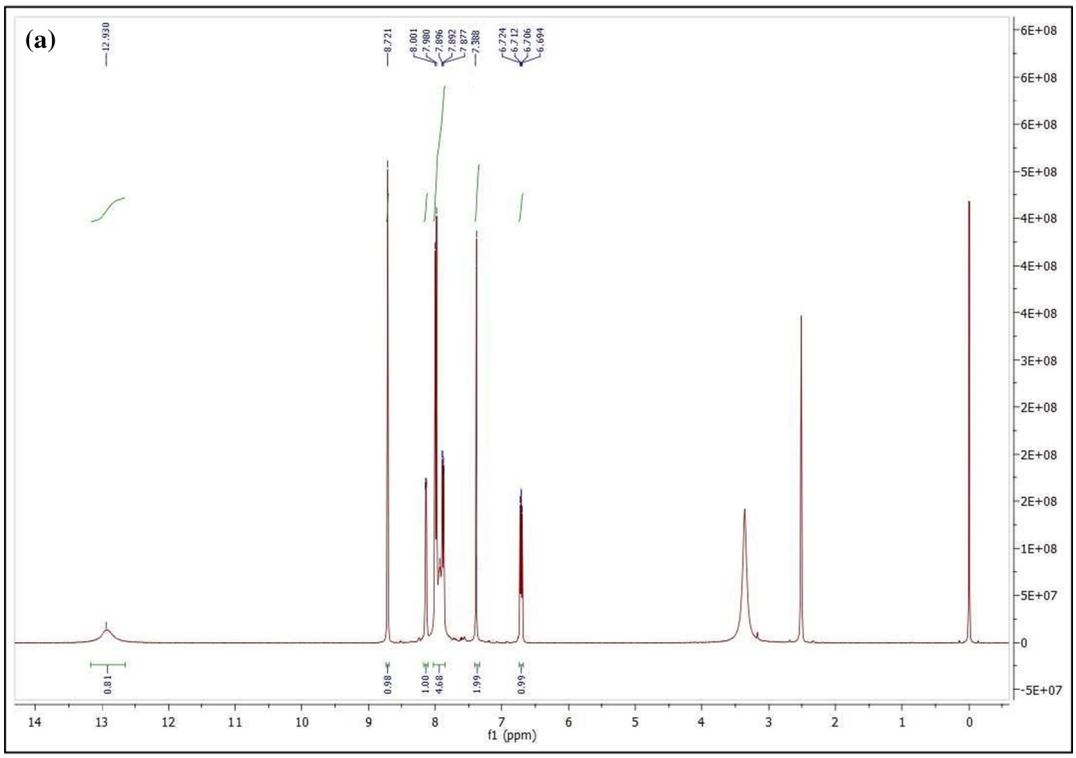
(a)
12.930
8.721
8.001
7.980
7.896
7.892
7.877
7.388
6.724
6.712
6.706
6.694
0.81
0.98
1.00
4.68
1.99
0.99
f1 (ppm)

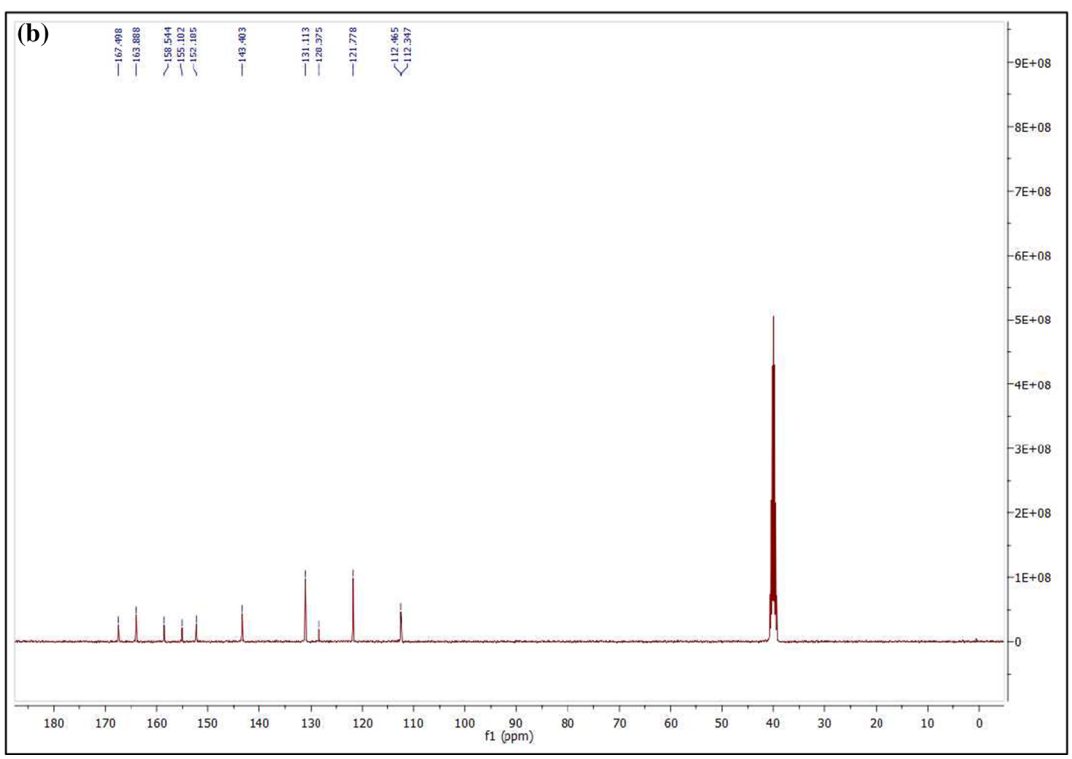
(b)
167.498
163.888
158.544
155.102
152.185
143.403
131.113
126.375
121.778
112.465
112.347
f1 (ppm)

◀**Fig. 2** **a** ^{1}H NMR and **b** ^{13}C NMR spectrum of the ligand (**L**)

response of compounds in presence of an applied electric field to predict cross-section of various scattering processes, molecular interactions and NLO properties of the system (Meyers et al. 1994; Hinchliffe and Munn 1985). β_t is a third rank tensor. Therefore, it was measured as a 3 × 3 × 3 matrix. From the basis of Kleinman symmetry (Kleinman 1962), all the 27 components were condensed to ten components indicated as β_{xxx}, β_{xxy}, β_{xyy}, β_{yyy}, β_{xxz}, β_{xyz}, β_{yyz}, β_{xzz}, β_{yzz}, β_{zzz}. So, by using these components X, Y, Z we can calculate the μ_t, α_t and β_{tot} by the following equations.

$$\mu = \mu_x^2 + \mu_y^2 + \mu_z^2 \tag{1}$$

$$\alpha_o = \frac{\alpha_{xx} + \alpha_{yy} + \alpha_{zz}}{3} \tag{2}$$

$$\Delta\alpha = 2^{-1/2}[(\alpha_{xx} - \alpha_{yy})^2 + (\alpha_{yy} - \alpha_{xx})^2 + 6\alpha_{xx}^2]^{1/2} \tag{3}$$

$$\beta = (\beta_x^2 + \beta_y^2 + \beta_z^2)^{1/2} \tag{4}$$

$$\beta_x = \beta_{xxx} + \beta_{xyy} + \beta_{xzz} \tag{5}$$

$$\beta_y = \beta_{yyy} + \beta_{xxy} + \beta_{yzz} \tag{6}$$

$$\beta_z = \beta_{zzz} + \beta_{xxz} + \beta_{yyz} \tag{7}$$

In this work, α_t, β_t and μ_t were calculated using the DFT approach and the results are given in Table 7. It is usual practice to determine the NLO behavior of compounds by comparing its μ_t and β_t with corresponding values of urea, which are 1.3732 Debye and 0.3728×10^{-30} cm^5/ e.s.u, respectively. The calculated β_t value of the ligand is 16.962×10^{-30} cm^5/ e.s.u, which was 45 times greater than urea. Hence, the ligand exhibits NLO properties. The complexes **2**, **3** and **5** showed more first order hyperpolarizability values compared to the free ligand. The remaining complexes exhibited lesser first order hyperpolarizability values than the ligand. The non-linear optical activity was associated with the intra-molecular charge transfer, obtaining from the electron cloud movement through resonance (Arivazhagan and Jeyavijayan 2011). Hence, the ligand and its metal complexes **2**, **3** and **5** are strong candidates for the expansion of NLO materials. The components of first order hyperpolarizability were also helpful to understand charge delocalization of the compounds.

EPR spectral studies

EPR studies are performed to identify the number of unpaired electrons and type of the bonds between the ligand and its Cu(II) complexes. The EPR parameters are listed in Table 8 and Fig. 7. The EPR spectrum of the Cu(II) complex was recorded at room temperature and shows two bands, one of small intensity towards the low field and another one large intensity towards the high field. Based on these bands the values of $g_{\|}$ and $g_{\perp}$ have been calculated (Anees et al. 2019; Kneubuhl 1960). From the results, $g_{\|} = 2.22$ and the other to $g_{\perp} = 2.05$. i.e. $> g_{\|} g_{\perp}$, pointing out that metal ion contains its unpaired electron in its $d_{x^2-y^2}$ orbital, and suggests a square-planar geometry (Konakanchi et al. 2018a, b). Kivelson and Neimann 1961) showed that $g_{\|} > 2.3$ for ionic environment and < 2.3 for covalent compounds. From Table 8 that $g_{\|}$ obtained for the present complex is less than 2.3 indicating the covalent character of M–L band. According to Hathaway and Billing 1970), if the G value is larger than 4, the exchange interaction is negligible, whereas if its value is less than 4 indicates considerable interaction in solid complexes. In the present case G is found to be greater than 4, thus ruling out solid state exchange interactions between copper centers. Further comparison of $K^2{}_{\|}$ and $K^2{}_{\perp}$ values (Table 8) obtained points out that complex **3**, $K^2{}_{\|} > K^2{}_{\perp}$, suggest that out of plane pi-bonded (Konakanchi et al. 2018a, b). The spin–orbit coupling constant (λ) calculated using the relation.

$$g_{\|} = [2 - (8\lambda/10\,Dq)$$

The λ value for the complex **3** (− 442 cm^{-1}) is found to be much lower than the free ion value λ_0 (− 828 cm^{-1}) which supports covalent character (Kavitha et al. 2013).

(a)

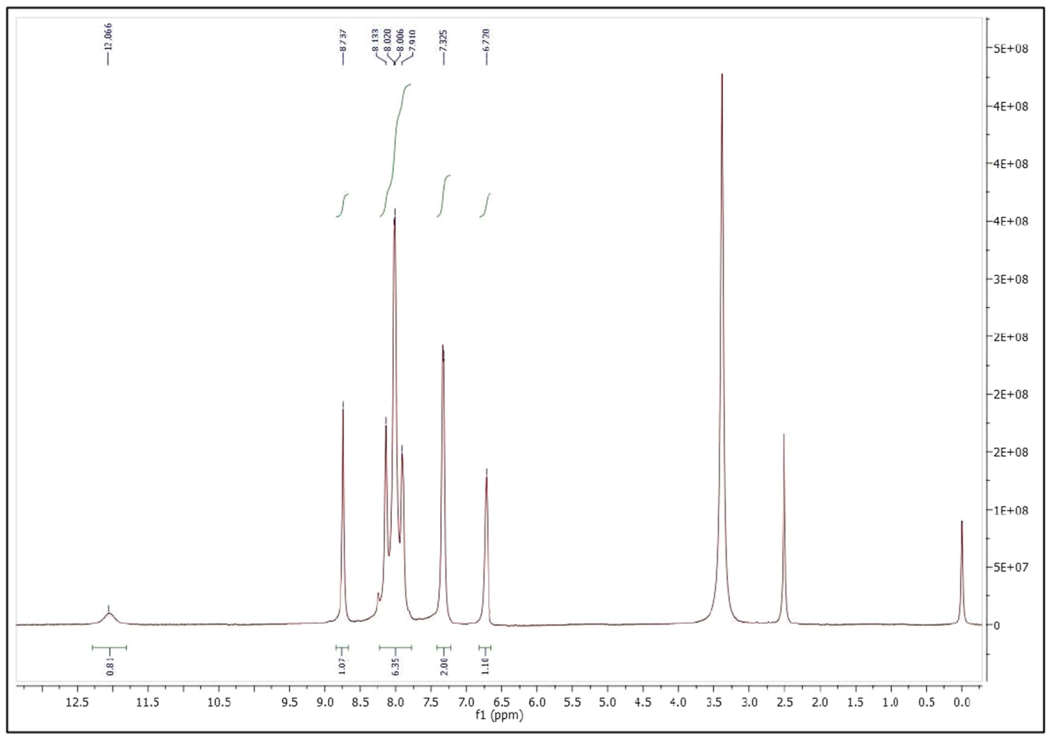
12.066
8.737
8.133
8.020
8.006
7.910
7.325
6.720
0.81
1.07
6.35
2.06
1.16
f1 (ppm)

(b)

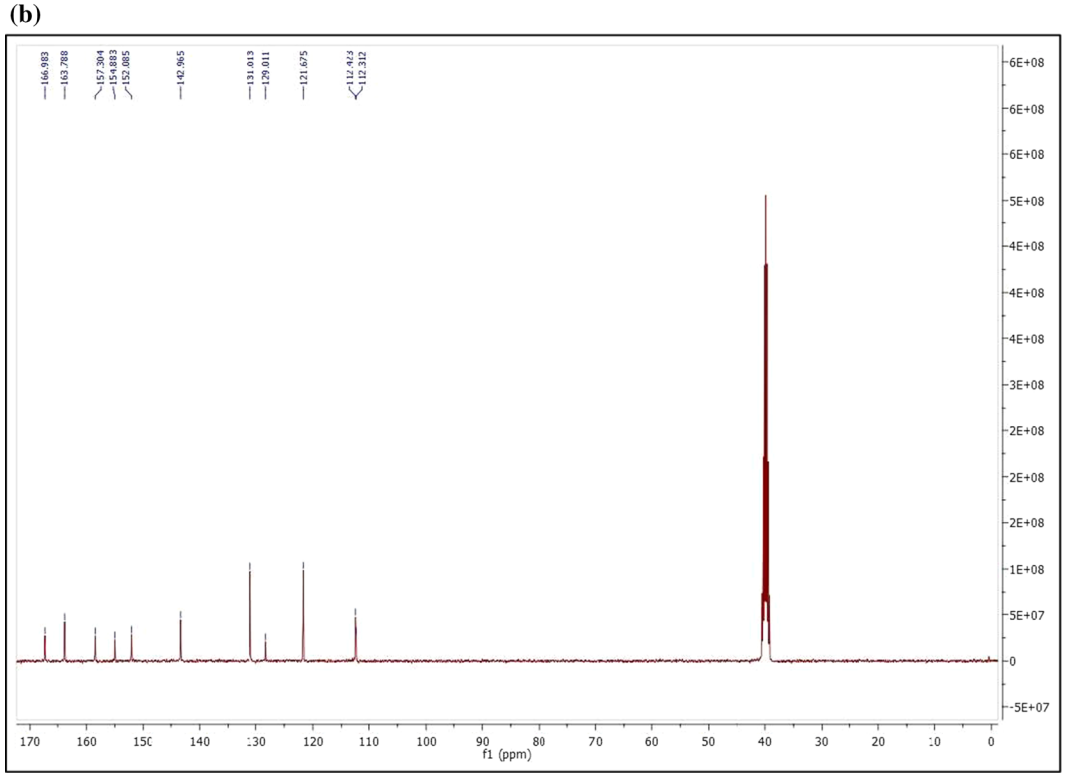
166.983
163.788
157.304
154.883
152.085
142.965
131.013
129.011
121.675
112.414
112.312
f1 (ppm)

◀ **Fig. 3** **a** ^{1}H NMR and **b** ^{13}C NMR spectrum of zinc(II) complex (**4**)

Biological evaluation

Antimicrobial screening

Microorganisms used in this work were three gram negative bacteria like *Proteus vulgaris*, *Klebsiella pneumoniae* and *Pseudomonas aeruginosa,* two gram positive bacteria like *Staphylococcus aureus* and *Bacillus subtilis* and few fungal strains like *Aspergillus niger*, *Aspergillus flavus*, *Curvularia lunata*, *Rhizoctonia bataticola* and *Candida albicans* by using disc diffusion method (Mallela et al. 2018; Arun et al. 2015). Streptomycin and Ketoconazole were chosen as reference drugs for bacteria and fungi, respectively. The MIC values of the tested compounds and reference drugs were expressed in µM. The results are present in Table 9 (antibacterial) and Table 10 (antifungal), respectively. From the results, the complex **3** exhibited excellent activity against S. *aureus* and *P. vulgaris* strains with MIC values of 4.21 and 8.18 µM, respectively and also these compunds showed significant activity against *B. subtilis* (MIC: 5.13 µM) and *P. aeruginosa* (MIC: 6.01 µM). The complex **5** exhibited broad spectrum activity against the strains with MIC values of 5.17 µM (S. *aureus*), 7.69 µg/mL (*B. subtilis*), 10.54 µM (*P. vulgaris*), 8.24 µM (*K. Pneumoniae*) and 7.25 µM (*P.aeruginosa*), respectively. Complex **4** against *B. Subtilis* (MIC: 11.50 µM), complex **2** against *P. vulgaris* (MIC: 21.01 µM) and complex **1** against *P.aeruginosa* (MIC: 10.91 µM) exhibited moderate activity compared to reference drug. The antifungal activity results are observed that the ligand is ineffective and it shows only marginal activity against the microorganisms tested. While complexes **2** and **3** have shown potent activity against *A. niger* (MIC = 3.94 µM) and *R. bataticola* (MIC = 6.24 µM), respectively compared to standard drug Ketoconazole. The complexes **3** and **5** exhibited significant activity against *A. niger* with MIC values of 4.17 and 40.3 µM, respectively. Complexes **1**, **2** and **3** against *C. albicans* showed good activity with MIC values of 7.12, 7.99 and 8.18 µM, respectively. Complex **2** against *A. flavus* (MIC = 10.77 µM) and complex **4** against *C. lunata* (MIC = 6.41 µM) registered moderate activity. In few of the complexes showed the same level of activity as the ligand. This difference might be due to their difference in Gram status.

Antioxidant activity

Antioxidant activity of the synthesized compounds has attracted a lot of interest and has been evaluated mostly in the in vitro systems (Sathyadevi et al. 2012; Mohanraj et al. 2016). The ligand and its metal complexes were investigated for their antioxidant ability and were carried out by using DPPH (1,1-diphenyl-2-picrylhydrazyl) radical as a reagent in the spectrophotometric test (Rohini et al. 2018a, b). Ascorbic acid is used as a reference antioxidant. The compounds were performed in triplicate and calculated the standard deviation (Gul et al. 2013). The IC_{50} (µM) values were given in Table 11 and Fig. 8. From the results, the complex **4** exhibited significant antioxidant activity with an IC_{50} value of 6.11 ± 0.54 µM compared to the reference drug showed their IC_{50} value of 4.61 ± 0.93 µM. Complex **1** exhibited good activity with IC_{50} value of 7.63 ± 1.57 µM. All the other complexes IC_{50} values in between 13.16 ± 0.85 µM and 29.47 ± 0.18 µM. According to the IC_{50} values the order of the ligand and its complexes are **4** > **1** > **2** > **3** > **5** > **L**.

In vitro antiproliferative evaluation

The successful evaluations of the antimicrobial and scavenging activity, we have also examined the anticancer evaluation against different cancer cell lines, IMR-32 (neuroblastoma), HeLa (cervical), MCF-7 (breast), A549 (lung), HepG-2 (liver) and HEK293 (embryonic kidney) by using 3-(4,5-dimethylthiazol-2-yl)-2,5-diphenyltetrazolium bromide (MTT) method (Mosmann 1983; Rohini et al. 2018a, b). The MTT assay results were shown in IC_{50}, expressed in micromolar units and summarized in Table 12. The percentage of cell viability *versus* concentration graphs is shown in Fig. 9. Cisplatin is used as a reference drug. The results clearly indicate that complex **4** showed excellent anti-proliferative activity against IMR-32, A549 and HepG-2 with an IC_{50} value of 7.81 ± 0.52 µM, 6.18 ± 1.15 µM and 15.28 ± 1.26 µM, respectively. Which are close to standard drug cisplatin (IC_{50} = 5.78 ± 0.12 µM,

(a)

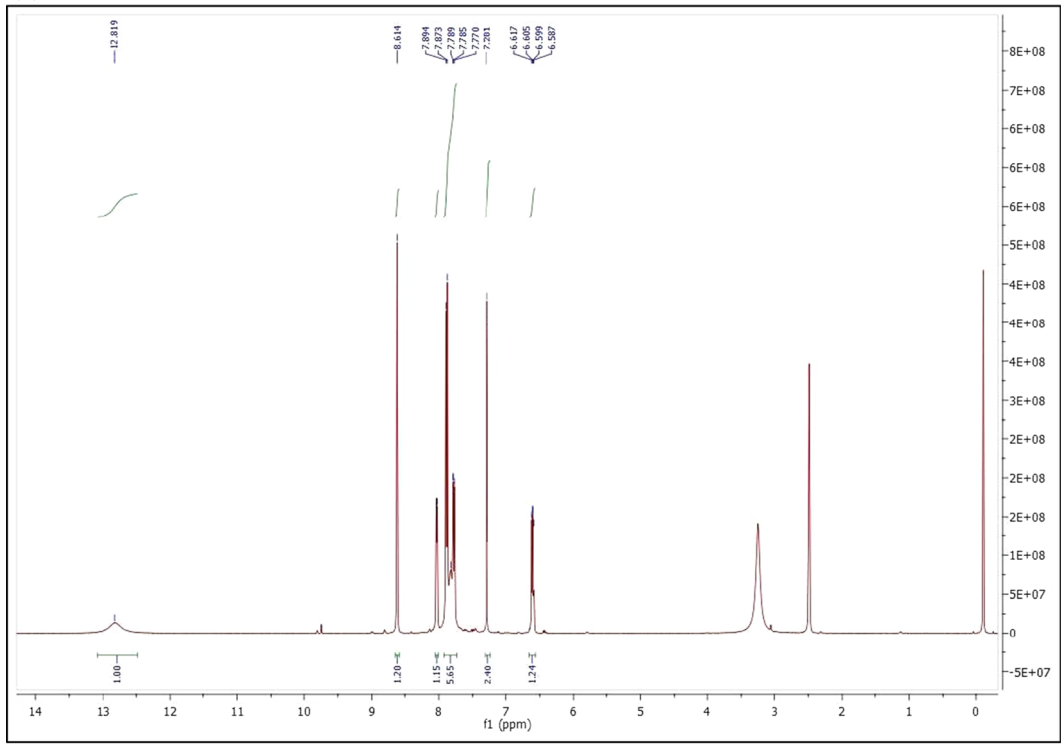
12.819
8.614
7.894
7.873
7.789
7.785
7.770
7.701
6.617
6.605
6.599
6.587
1.00
1.20
1.15
5.65
2.40
1.24
f1 (ppm)

(b)

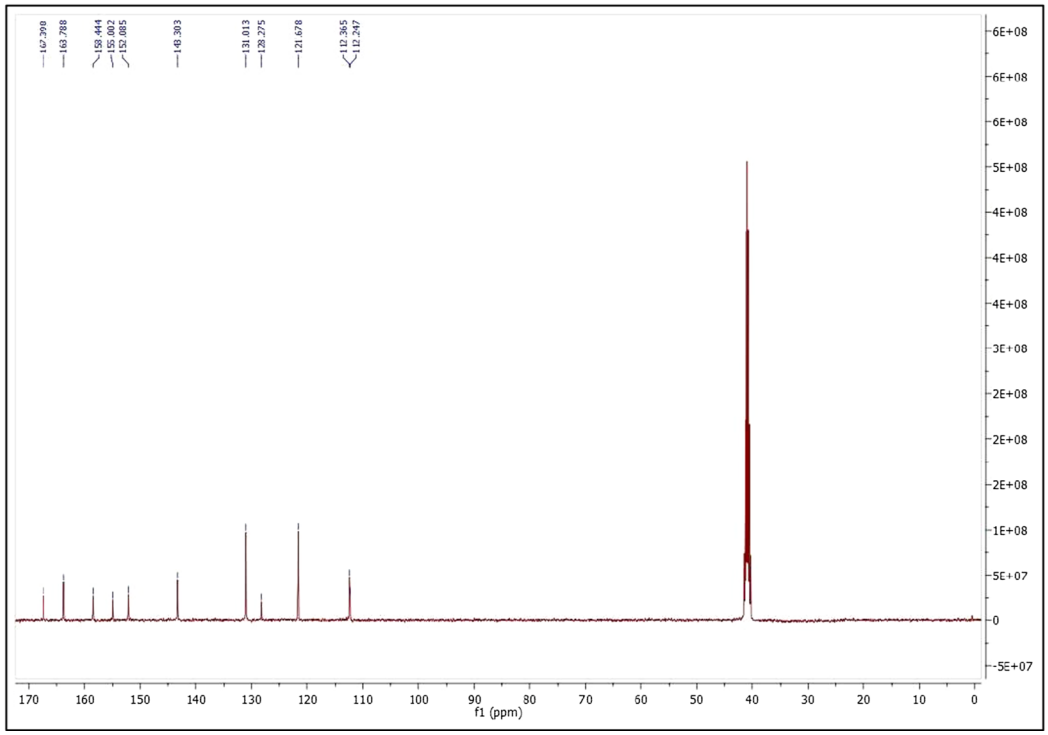
167.390
163.788
158.444
155.002
152.085
148.303
131.013
128.275
121.678
112.365
112.247
f1 (ppm)

◀**Fig. 4** **a** ^{1}H NMR and **b** ^{13}C NMR spectrum of palladium(II) complex (**5**)

4.90 ± 0.31 and 10.52 ± 0.40, respectively) and also the complex **4** showed good activity against MCF-7 (IC_{50} = 7.41 ± 0.32 µM) and HeLa (IC_{50} = 5.99 ± 0.23 µM), respectively. Similarly complex **1** exhibited potent with broad spectrum activity with IC_{50} values against HeLa (5.94 ± 1.13 µM), IMR-32 (8.51 ± 0.12 µM), HepG-2 (16.51 ± 1.18 µM), A549 (8.27 ± 0.38 µM) and MCF-7 (13.26 ± 0.19 µM). The observed higher efficiency of complexes **1** and **4** are may be due to the presence of ligand coordinated to central Cobalt and Zinc metal ions. Also complex **2** against HeLa (IC_{50} = 12.72 ± 0.27 µM) and **L** against A549 (IC_{50} = 19.38 ± 1.07 µM) exhibited moderate activity. The other compounds exhibited the least activity against the cell lines. In addition, we have also tested the cytotoxicity of the potent compounds **1** & **4** against normal cancer cell line HEK293 with IC_{50} values of 96.57 ± 0.42 µM and 81.37 ± 0.10 µM, respectively. None of the potent complexes (**1** and **4**) interrupted the viability of the normal cell line, suggesting that the potent compounds are not toxic.

Molecular docking

The in silico molecular docking analysis of the ligand and its metal complexes against human epidermal growth receptor (HER2) and epidermal growth factor (EGFR) was carried out to verify the relation between the in vitro antiproliferative activity results and

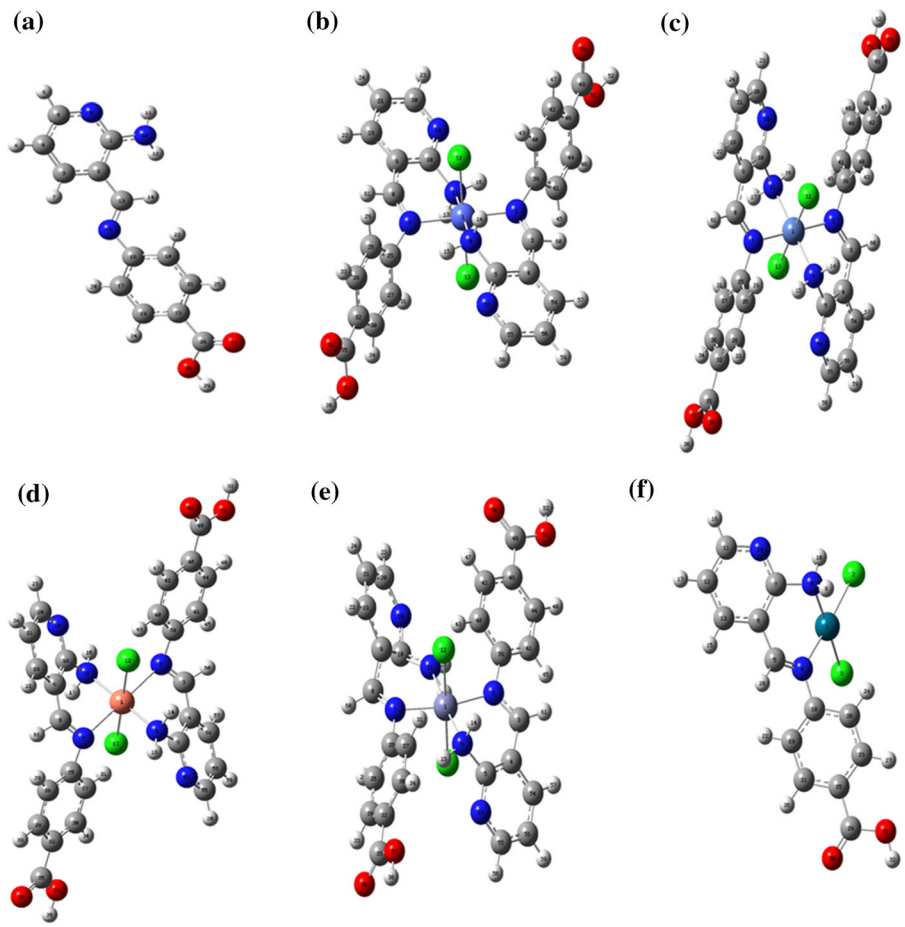

Fig. 5 Optimized structures along with atomic numbering of **a** ligand, **b** complex **1**, **c** complex **2**, **d** complex **3**, **e** complex **4** and **f** complex **5**

Table 4 Optimized geometry parameters of ligand (**L**)

Bond length	Value (Å)	Bond angle	Value (°)	Dihedral angle	Value (°)
C1–C2	1.42122	C1–C2–C3	117.21480	C1–C2–C3–C4	− 1.75184
C2–C3	1.39995	C2–C3–C4	120.27239	C2–C3–C4–C5	− 0.45624
C3–C4	1.38588	C3–C4–C5	117.63683	C3–C4–C5–N6	1.91374
C4–C5	1.39556	C4–C5–N6	123.85376	C4–C5–C6–C1	− 0.91487
C5–N6	1.33104	C5–N6–C1	118.55648	C5–N6–C1–C2	− 1.54473
N6–C1	1.34098	N6–C1–C2	122.39875	N6–C1–C2–C3	2.84768
C3–H7	1.08346	C1–C2–C13	121.81121	C2–C3–C4–H7	− 178.91721
C4–H8	1.08244	C2–C13–H14	116.88223	C3–C4–C5–H8	− 179.00745
C5–H9	1.08661	C2–C13–N15	122.70621	C4–C5–N6–H9	179.66909
C1–N10	1.37990	C13–N15–C16	120.12913	C2–C1–N6–N10	178.14106
N10–H11	1.00981	N15–C16–C17	118.08140	C2–C6–N10–H12	31.02831
N10–H12	1.00683	C16–C17–C19	120.56235	N6–C1–N10–H11	− 10.65379
C2–C13	1.46032	C17–C19–C23	120.28755	C1–C2–C13=N15	− 169.38350
C13–H14	1.09707	C19–C23–C21	119.32780	C2–C13=N15–C16	− 174.81323
C13=N15	1.28063	C23–C21–C18	120.51530	N15–C26–C17–C19	− 179.71188
N15–C16	1.39967	C21–C18–C16	120.30906	C16–C17–C19–C23	1.51244
C16–C17	1.40447	C18–C16–C17	118.95816	C17–C19–C23–C21	0.12311
C17–C19	1.38617	C16–C17–H20	118.56143	C19–23–C21–C18	− 0.82620
C19–C23	1.40246	C17–C19–H24	120.10095	C23–C2–C18–C16	− 0.10306
C23–C21	1.39970	C23–C21–H25	118.76452	C21–C18–C16–C17	1.70937
C21–C18	1.38711	C21–C18–H22	119.96215	C18–C16–C17–C19	− 2.41612
C18–C16	1.40679	C19–C23–C26	122.40065	C16–C17–C19–H20	− 179.35360
C17–H20	1.08330	C23–C26=O27	125.22327	C17–C19–C23–H24	179.43723
C19–H24	1.08215	C23–C26–O28	113.07488	C23–C21–C18–H25	179.45454
C21–H25	1.08323	C26–O28–H29	106.54015	C21–C18–C16–H22	177.90932
C18–H22	1.08387	O27–C26–O28	121.70174	C19–C23–C26–O28	0.62241
C23–C26	1.48157	H14–C13=N15	120.40763	C2–C23–C26=O27	− 0.26012
C26=O27	1.21031	C2–C1–N10	122.49422	C23–C26–O28–H29	− 179.96170
C26–O28	1.35995	C1–N10–H12	119.07478	–	–
O28–H29	0.96819	C1–N10–H11	113.62942	–	–

binding affinities of the inhibitors by using auto dock program. It plays a major role in malignant growth from various origins (Jost et al. 2013). It is expressed on the surfaces of most of the cells of human body (Jost et al. 2013). The overexpression of the HER2 involved in several cancers like breast, adenocarcinoma of lungs, stomach (Buza et al. 2014), ovarian (Santin et al. 2008), uterine cancers (Buza et al. 2014; Santin et al. 2008) etc., It is a suitable target for kinase inhibitors (Jost et al. 2013). On the other hand, EGFR is the prominent cell-surface receptor and belongs to the EGFR family (Sebastian et al. 1998). The TKD (tyrosine kinase domain) and extracellular mutations of EGFR causes non small cell lung cancer and glioblastoma respectively (Foloppe and MacKerell 2000; Breneman and Wiberg 1990; Walker et al. 2009). Its overexpression also leads to epithelial tumors of the head, neck and anal cancer (Lynch et al. 2004; Davis and Teague 1999). By considering the aforementioned reasons, we have chosen the target protein receptors HER2 and EGFR for the docking studies. Herein, the main aim is to explore the binding

Table 5 Selected bond lengths and bond angles of the complexes (**1–5**)

1		2		3		4		5	
Bond length	Value (Å)	Bond length	Value (Å)	Bond length	Value (Å)	Bond length	Value (Å)	Bond length	Value (Å)
Co1–N2	2.03218	Ni1–N2	2.30606	Cu1–N2	2.35000	Zn1–N2	1.91254	Pd1–Cl2	2.35353
N2–C3	1.25976	N2–C3	1.27349	N2–C3	1.11398	N2–C3	1.30598	Pd1–Cl3	2.35015
C3–C4	1.44058	C3–C4	1.46220	C3–C4	1.37670	C3–C4	1.46406	Pd1–N4	2.07926
C4–C5	1.42907	C4–C5	1.42019	C4–C5	1.43970	C4–C5	1.41436	N4–C5	1.31025
C5–N6	1.47725	C5–N6	1.45039	C5–N6	1.46491	C5–N6	1.54326	C5–C6	1.46658
N6–Co1	2.00350	N6–Ni1	1.96345	N6–Cu1	1.92265	N6–Zn1	2.06224	C6–C7	1.42277
Co1–N2	2.03915	Ni1–N7	2.31058	N7–Cu1	2.33000	N7–Zn1	2.45651	C7–N8	1.44905
N7–C8	1.26117	N7–C8	1.27292	N7–C8	1.11757	N7–C8	1.52726	N8–Pd1	2.10592
C8–C9	1.44408	C8–C9	1.46166	C8–C9	1.37729	C8–C9	1.61935	Bond angle	Value (°)
C9–C10	1.42799	C9–C10	1.42012	C9–C10	1.43970	C9–C10	1.45384	Cl2–Pd1–Cl3	93.43178
C10–N11	1.48072	C10–N11	1.45018	C10–N11	1.46706	C10–N11	1.48986	Cl3–Pd1–N4	92.73289
C11–Co1	2.00790	N11–Ni1	1.96451	N11–Cu1	1.93074	N11–Zn1	1.92163	Pd1–N4–C5	121.26035
Co1–Cl12	2.27016	Ni1–Cl12	2.29934	Cu1–Cl12	2.16467	Zn1–Cll2	2.29848	N4–C5–C6	125.87500
Co1–Cl13	2.28411	Ni1–Cl13	2.29944	Cu1–Cl13	2.16388	Zn1–Cll3	2.28958	C5–C6–C7	124.58417
								C6–C7–N8	120.56767
								C7–N8–Pd1	112.52592
								N8–Pd1–Cl2	85.61200
								N8–Pd1–N4	88.21715

Bond angle	Value (Å)	Bond angle	Value (Å)	Bond angle	Value (Å)	Bond angle	Value (Å)
Co1–N2–C3	111.64135	Ni1–N2–C3	119.58391	Cu1–N2–C3	100.05199	Zn1–N2–C3	123.34310
N2–C3–C4	142.99340	N2–C3–C4	126.55903	N2–C3–C4	138.89470	N2–C3–C4	123.78851
C3–C4–C5	115.68172	C3–C4–C5	124.07261	C3–C4–C5	123.35645	C3–C4–C5	128.93135
C4–C5–C6	119.35257	C4–C5–N6	121.01749	C4–C5–N6	121.34667	C4–C5–C6	121.95938
C5–C6–Co1	118.62623	C5–N6–Ni1	119.20823	Cu1–N7–C8	100.29560	C5–N6–Zn1	109.94615
Co1–N7–C8	111.65681	Ni1–N7–C8	119.45140	N7–C8–C9	138.75878	Zn1–N7–C8	99.63015
N7–C8–C9	143.07162	N7–C8–C9	126.62006	C8–C9–C10	123.21746	N7–C8–C9	134.60675
C8–C9–C10	115.57772	C8–C9–C10	123.92696	C9–C10–N11	121.23341	N8–C9–C10	98.91166
C9–C10–N11	119.19665	C9–C10–N11	120.95988	C10–N11–Cu1	101.77903	C9–C10–N11	120.17000
C10–N11–Co1	119.30108	C10–N11–Ni1	119.11235	N2–Cu1–Cl12	76.70180	C10–C11–Zn1	119.84187
N2–Co1–Cl12	91.87577	N2–Ni1–Cl12	91.59393	N6–Cu1–Cl12	92.18965	N2–Zn1–Cl12	85.26809
N6–Co1–Cl12	86.81401	N6–Ni1–Cl12	85.80806	N7–Cu1–Cl13	77.89497	N7–Zn1–Cl12	83.27208
N7–Co1–Cl13	91.57108	N7–Ni1–Cl13	91.32768	N11–Cu1–Cl13	91.76743	N6–Zn1–Cl13	93.94000
N11–Co1–Cl13	87.35005	N11–Ni1–Cl13	85.84111	–	–	N11–Zn–Cl13	81.34695

behaviour (in terms of Binding energy) of the target compounds against HER2 and EGFR and their results were compared with well established inhibitors (in vitro and in vivo) such as Canertinib (HER2), Afatinib (HER2), Lapatinib (EGFR) and Gefitinib (EFGR) (Schroeder et al. 2014). The comparative docking studies of the compounds [ligand and its metal complexes (**1–5**)] and the reported inhibitors (Canertinib, Afatinib, Lapatinib and Gefitinib) against the proteins HER2 and EGFR along with their corresponding binding energies, which were listed in Table 13. As shown in Table 13, docking results

Table 6 Frontier molecular orbital parameters of ligand (**L**) and its metal complexes (**1–5**)

Frontier molecular orbital parameter	1	2	3	4	5	L
HOMO energy	− 7.12383	− 7.82452	− 7.57527	− 5.50614	− 4.84491	− 9.05255
LUMO energy	− 6.30424	− 6.80982	− 5.95158	− 5.01199	− 3.83511	− 6.26097
Frontier molecular orbital energy gap	**0.81958**	**1.01470**	**1.62368**	**0.49415**	**1.00979**	**2.79157**
Ionization energy (I)	7.12383	7.82452	7.57527	5.50614	4.84491	9.05255
Electron affinity (A)	6.30424	6.80982	5.95158	5.01199	3.83511	6.26097
Global hardness (η)	0.40979	0.50735	0.81184	0.24707	0.504896	1.39578
Chemical potential (μ)	− 6.71403	− 7.31717	− 6.76342	− 5.25906	− 4.34001	− 7.65676
Global electrophilicity index (ω)	55.00158	52.76531	28.17294	55.96903	18.65302	21.00117

Bold indicates compared with the standard drug that particular complexes exhibited good activity

[Values present (**eV**)]

revealed that complexes **1** and **4** showed the least binding energies compared to other metal complexes against receptors HER2 and EGFR with their binding energies − 7.31, − 6.46 kcal/mol (for complex **1**); − 8.02, − 7.35 kcal mol^{-1} (for complex **4**), respectively. Hence HER2 and EGFR were taken as the target protein receptors for the insightful deep discussion for complexes **1** and **4**. The best docking poses of the complexes **1** and **4** were shown in Figs. 10 and 11 the molecular docking results for the complex **1** against HER2 exhibited four hydrogen bonds; one strong hydrogen bond in between the OH group of carboxylic acid moiety and the amino acid residue LYS875 with bond length 1.80 Å, one hydrogen bond in between an amino group of 2-aminopyridyl ring and amino acid residue SER720 with bond length 2.28 Å, one hydrogen bond in between OH group of benzoic acid moiety and the amino acid residue ALA722 with bond length 2.90 Å and one carbon–hydrogen bond in between –CH group of pyridyl ring and amino acid residue GLY724 with bond length 3.03 Å. The pyridyl ring interacts with the amino acid residues ARG841 and CYS797 and the phenyl ring of the benzoic acid moiety interacts with amino acid residue ALA722 through hydrophobic interactions. In relation the complex **1** against EGFR exhibited eight hydrogen bonds; one strong hydrogen bond in between -O-atom of carboxylic acid moiety and the amino acid residues ARG817 and GLY697 with bond length 1.87 Å and 3.28 Å respectively, one hydrogen bond in between H-atom of the carboxylic acid moiety and the amino acid residue ASP813 with bond length 2.14 Å, one hydrogen bond in between carbonyl oxygen atom of the carboxylic acid group and the amino acid residue LYS721 with hydrogen bond length 3.04 Å, one hydrogen bond in between amino group of 2-aminopyridyl ring and amino acid residue ARG817 with bond length 2.08 Å, one hydrogen bond in between N-atom of pyridyl ring and the amino acid residue CYS773 with bond length 2.87 Å and one carbon-hydrogen bond in between –CH group of pyridyl ring and amino acid residue ASP831 with bond length 3.16 Å, one hydrogen bond in between N-atom of the imine group and the amino acid residue ARG817. The pyridyl ring interacts with the amino acid residues LEU820, ARG817 and VAL702 and the phenyl ring of the benzoic acid moiety interact with amino acid residue ARG817 through hydrophobic interactions. The hydrogen bonding interactions and hydrophobic interactions of the complex **1** was shown in Figs. 10 and 11.

In case of complex **4** against HER2 exhibited five hydrogen bonds; one strong hydrogen bond in between the –OH group of benzoic acid moiety and amino acid residue PRO877 with bond length 1.69 Å, one strong hydrogen bond in between the –OH group of benzoic acid moiety and amino acid residue ASP837 with bond length 1.85 Å, one hydrogen bond in between –CH group of imine moiety with amino acid residue ALA722 with bond length 3.56 Å, one hydrogen bond in between –CH group of pyridyl moiety with amino acid residue GLY719 with bond length 3.69 Å and one hydrogen bond in between carbonyl group of benzoic moiety with amino acid residue PRO877 with bond length 3.77 Å. The pyridyl ring interacts with the amino acid residues ARG841, LYS745 and VAL726 through hydrophobic interactions. In addition to this,

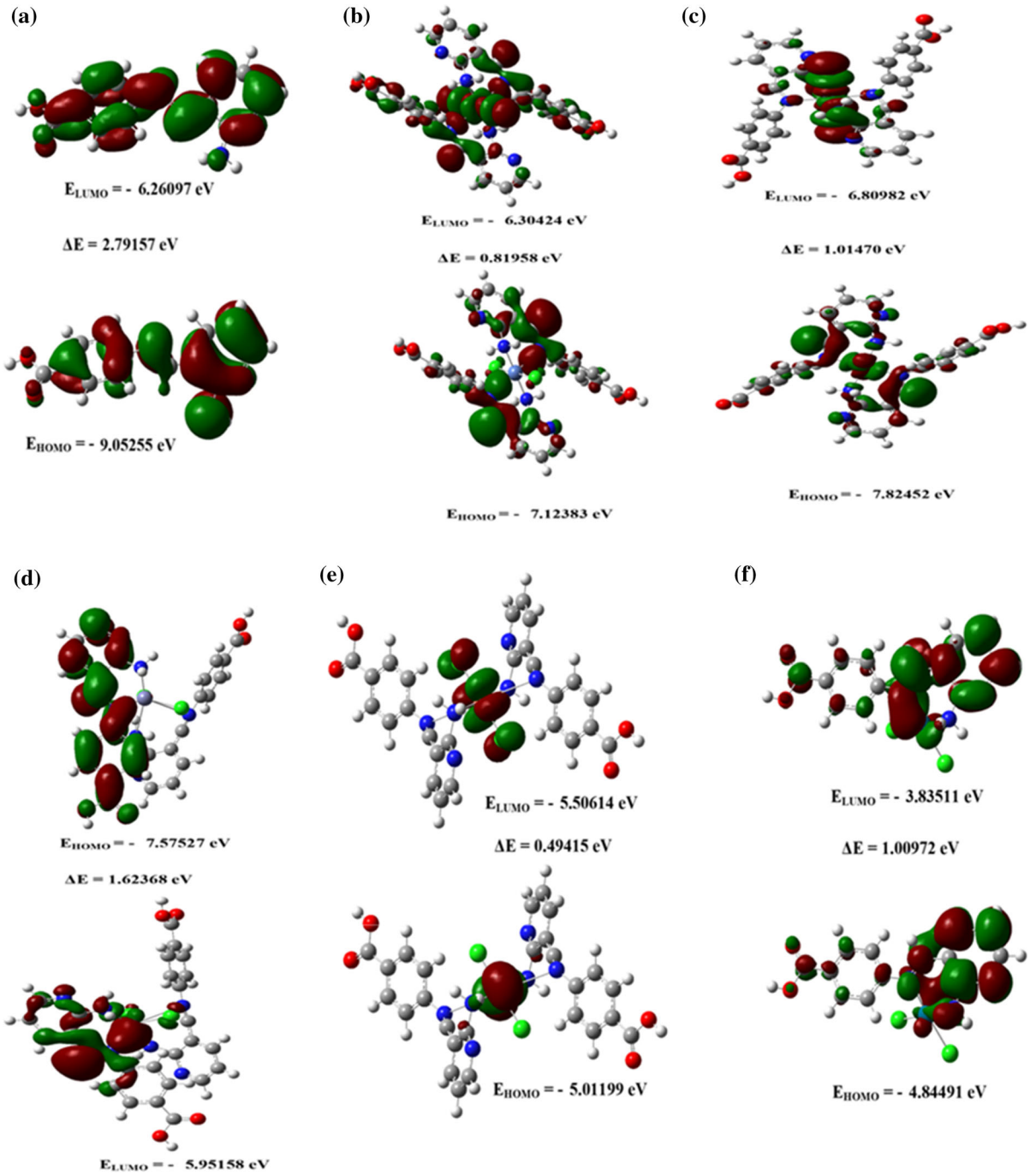

Fig. 6 Frontier molecular orbitals of **a** ligand, **b** complex **1**, **c** complex **2**, **d** complex **3**, **e** complex **4** and **f** complex **5**

there was an electrostatic interaction between the pyridyl moiety with the amino acid residues ASP855 and CYS797. In relation the complex **4** against EGFR exhibited eight hydrogen bonds; three hydrogen bonds in between carbonyl oxygen atom of the carboxylic acid group and the amino acid residue ARG779, LYS851 and LYS889 with hydrogen bond lengths 1.93 Å, 1.95 Å and 3.37 Å respectively, one strong hydrogen bond in between the –OH group of benzoic acid moiety and amino acid residue LYS889 with

Table 7 The dipole moment (in Debye), polarizability and first order hyperpolarizability (in 10^{-30} cm^5/e.s.u) values of ligand and its metal complexes (**1–5**)

Type of component	1	2	3	4	5	L
β_{xxx}	35.1312	1412.5682	− 437.8606	116.6001	− 659.5690	− 2215.2291
β_{xxy}	− 87.0246	− 1177.8671	− 241.1182	19.3886	737.6800	− 3.2906
β_{xyy}	39.0115	− 624.5487	− 1023.0287	− 39.9696	51.2647	159.2177
β_{yyy}	− 149.7493	− 645.5117	− 1755.5558	− 5.5846	1793.0766	− 155.2760
β_{xxz}	− 34.0008	− 308.9618	31.8476	16.1393	− 177.4568	− 6.5763
β_{xyz}	− 14.1808	− 14.7839	19.7664	− 14.5895	28.5835	− 8.3224
β_{yyz}	36.1939	296.8233	447.3902	− 9.1699	− 114.7129	− 31.5628
β_{xzz}	0.7827	− 37.6109	− 16.9262	− 8.3271	− 127.2958	103.1029
β_{yzz}	0.5283	8.3044	89.1589	− 7.4804	84.9524	− 42.6507
β_{zzz}	0.3429	− 34.6800	65.0474	− 18.8521	− 201.0856	7.4817
β_t	2.141 × 10^{-30} cm^5/**e.s.u**	17.399 × 10^{-30} cm^5/e.s.u	21.347 × 10^{-30} cm^5/e.s.u	0.7048 × 10^{-30} cm^5/e.s.u	23.876 × 10^{-30} cm^5/e.s.u	16.962 × 10^{-30} cm^5/e.s.u
μ_x	0.4443	− 4.3181	0.8809	− 0.0019	− 2.0877	1.7981
μ_y	− 2.0118	− 4.8734	− 1.1144	− 0.7539	12.0509	− 0.5068
μz	− 1.1451	0.8624	− 2.7097	− 2.5866	− 4.6024	− 1.6375
μ_t	2.3571	6.5681	3.0595	2.6943	13.0676	2.4848
α_{xx}	597.2192	576.2061	608.3871	672.9969	364.6869	356.8497
α_{xy}	28.7435	− 105.6276	− 67.3388	17.6290	− 25.5022	− 4.4959
α_{yy}	545.8433	410.5628	526.1094	591.4939	242.7347	170.6526
α_{xz}	− 19.4824	22.6534	0.5215	10.0580	8.01807	− 5.0951
α_{yz}	32.9112	39.5342	− 34.6070	− 8.2554	23.4425	− 3.9852
α_{zz}	172.4103	259.2901	280.3167	274.8413	136.4581	115.5721
α_t	438.480	286.040	471.5960	513.1060	247.953	214.3530

Table 8 ESR spectral data of Cu(II) complex (**3**)

Complex	$g_{\parallel}$	$g_{\perp}$	g	G	$A_{\parallel} \times 10^5$ (cm^{-1})	$K^2{}_{\parallel}$	$K^2{}_{\perp}$	$-\lambda$
Cu(II) (**3**)	2.22	2.05	2.11	4.56	465	0.534	0.468	442

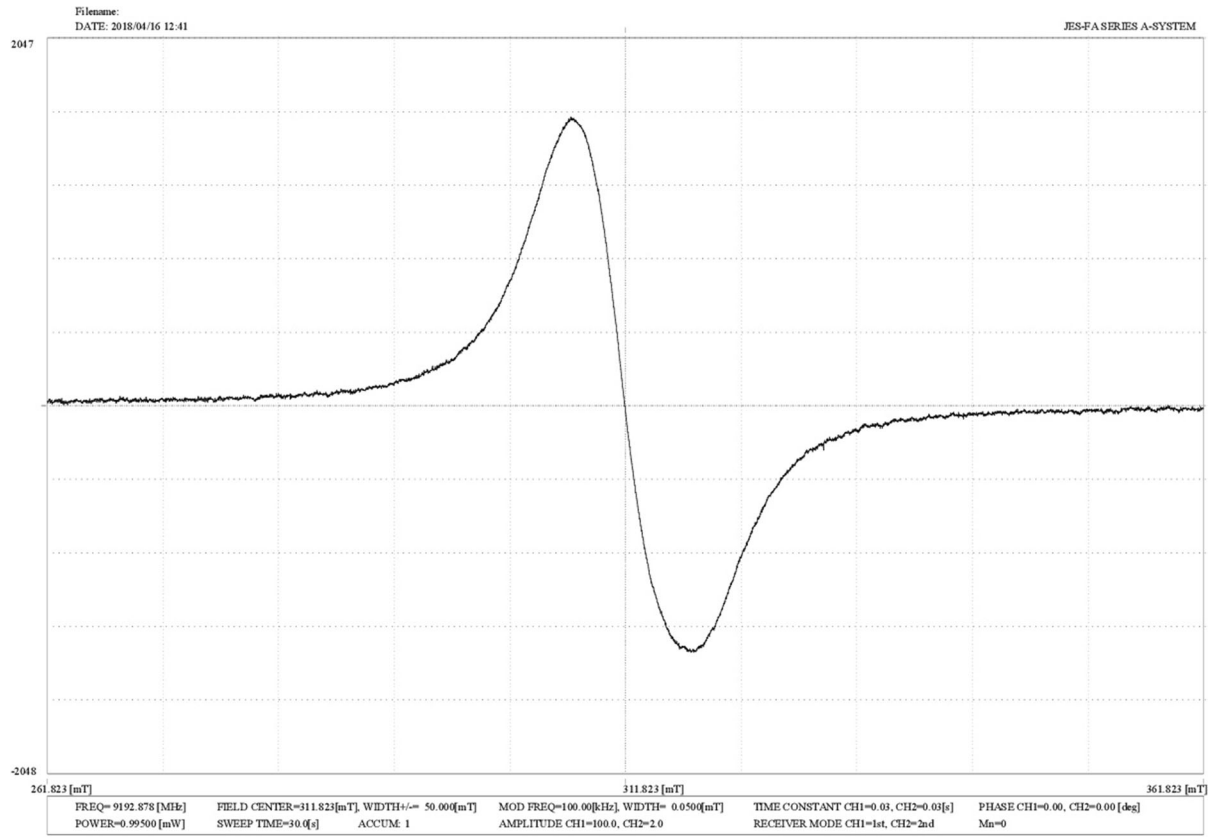

Fig. 7 ESR spectrum of copper(II) complex (**3**)

bond length 2.98 Å, two hydrogen bonds in between an amino group of 2-aminopyridyl ring and amino acid residue SER696 with bond length 1.61 Å, and 1.92 Å, one hydrogen bond in between *N*-atom of pyridyl ring with amino acid residue GLY695 with bond length 3.57 Å and One Pi-donor hydrogen bond in between pyridyl ring and amino acid residue SER696 with bond length 2.97 Å. The pyridyl ring interacts with the amino acid residues ARG817 through hydrophobic interactions. The hydrophobic interactions also played a vital role in increasing the affinity in between the synthesized compounds and targeted proteins. The hydrogen bonding interactions and hydrophobic interactions of the complex **4** was shown in Figs. 12 and 13. Finally, the docking results clearly suggest the affinity of the synthesized compounds (**1–5** and ligand) towards the protein receptor HER2 is better than that of the protein receptor EGFR. The docking results were quite consistent with experimental anticancer activity. The best docking poses of the standard compounds against the proteins HER2 and EGFR were included in the supplementary file (Figs. S1, S2).

Conclusion

In summary, the complexes (**1–5**) with Schiff base ligand has been designed, synthesized and characterized, further with an aim to evaluated for their antioxidant, antimicrobial, cytotoxic activity, DFT

Table 9 MIC of the synthesized compounds against the growth of bacteria

Compound	Minimum inhibitory concentration (μM)				
	S. aureus	*B. subtilis*	*P. vulgaris*	*K. pneumoniae*	*P. aeruginosa*
1	21.87	25.79	> 100	30.79	**10.91**
2	18.15	14.35	21.01	> 100	24.86
3	**4.21**	**5.13**	**8.18**	8.27	**6.01**
4	> 100	11.50	29.28	31.40	29.63
5	**5.17**	**7.69**	**10.54**	8.24	**7.25**
L	50	> 100	42.52	35.33	38.94
Streptomycin	3.42	3.15	6.25	3.15	4.27

Table 10 MIC of the synthesized compounds against the growth of fungi

Compound	Minimum inhibitory concentration (μM)				
	A. niger	*A. flavus*	*C. lunata*	*R. bataticola*	*C. albicans*
1	> 100	17.25	50	50	7.12
2	**3.94**	10.77	21.44	> 100	7.99
3	**4.17**	> 100	26.45	**6.24**	8.18
4	19.24	> 100	6.41	> 100	21.73
5	**4.03**	18.72	> 100	26.49	> 100
L	> 100	27.45	> 100	35.29	21.05
Ketoconazole	2.92	3.85	2.16	4.57	3.26

calculations and HER2, EGFR target based in silico docking studies. The metal–ligand stoichiometry in the complexes (**1–4**) corresponds to 1:2, in the case of Pd 1:1 stoichiometry, wherein ligand behaves in a bidentate manner towards metals coordinating through azomethine nitrogen atom and nitrogen of amine group. Based on different experimental evidences, the complexes ensured that the octahedral geometry have been proposed for complexes **1**, **2** and **4**, square planar for complexes **3** and **5**. All the complexes show non-electrolytic nature in DMF. The evaluation of ESR parameters from the ESR spectra confirms the M–L bonds are covalent and out of plane π-bonded. From the antimicrobial activity results, it is known that the metal complexes exert higher effectiveness compared to the ligand indicating that the metals are actually in action. Especially, complex **3** has shown excellent antimicrobial activity, complex **5** exhibited broad spectrum antibacterial activity, and complex **2** has shown superior antifungal activity compared to the standards streptomycin and ketoconazole. Antioxidant properties of the compounds, the compound **4** has shown very good activity compared to reference drug ascorbic acid. In Addition, complexes **4** and **1** showed potent anti-proliferative activity against IMR-32 (IC_{50} = 7.81 ± 0.52, 8.51 ± 0.12 μM), A549 (IC_{50} = 6.18 ± 1.15, 8.27 ± 0.38 μM) and HepG-2 (IC_{50} = 15.28 ± 1.26, 16.51 ± 1.18 μM), respectively. The docking results revealed that complexes 1 and 4 showed least binding energies against receptors HER2 and EGFR with their binding energies − 7.31, − 6.46 kcal/mol (for complex **1**); − 8.02, − 7.35 kcal mol^{-1} (for complex **4**), respectively compared to Canertinib (HER2), Afatinib (HER2), Lapatinib (EGFR) and Gefitinib (EFGR). From the results, it is clear that the complexes are strongly bound to HER2 and EGFR protein receptors. Interestingly, these compounds showed the most potent

Table 11 Antioxidant activity of the ligand and its metal complexes

Compounds	IC_{50} (μM)
1	**7.63 ± 1.57**
2	13.16 ± 0.85
3	20.96 ± 1.82
4	**6.11 ± 0.54**
5	22.89 ± 1.26
L	29.47 ± 0.18
Ascorbic acid	4.61 ± 0.93

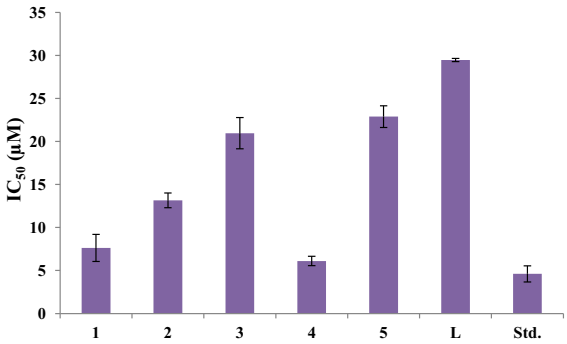

Fig. 8 Antioxidant activity of the ligand and its metal complexes (**1–5**)

anticancer activity and minimum binding energies obtained by the docking study. The results indicate that in silico molecular docking studies were well correlated with the experimental anti-proliferative activity results.

General considerations

All chemicals and solvents used in these investigations were purchased from Sigma Aldrich and Spectrochem as high purity materials. The infrared spectra of the samples were recorded using a PerkinElmer 100S FTIR spectrometer. The absorption spectra of compounds in DMF were performed from Perkin-Elmer UV–Visible Spectrophotometer. The molar conductivity measurements of the complexes in DMF were made at 10^{-3} M concentration. NMR spectra were recorded in DMSO solvent using TMS as an internal standard on a Brukner 400 MHz spectrometer. Analytical data for the compounds were obtained from the Vario EL − III CHNS analyzer. The Electron paramagnetic spectrum of the copper complex is recorded by using JOEL X-Band ESR spectrometer.

Table 12 Cytotoxic activity of the newly synthesized compounds on human cancer cell lines IMR-32, HeLa, MCF-7, A549 and HepG-2 [in vitro (IC_{50} μM)]

Compound	IMR-32	HeLa	MCF-7	A549	HepG-2	HEK 293
1	**8.51 ± 0.12**	**5.94 ± 1.13**	10.26 ± 0.19	**8.27 ± 0.38**	**16.51 ± 1.18**	**96.57 ± 0.42**
2	40.21 ± 1.25	12.72 ± 0.27	39.98 ± 1.34	34.87 ± 1.19	71.26 ± 1.92	ND
3	42.08 ± 0.61	39.08 ± 0.13	51.52 ± 1.12	43.13 ± 0.15	69.94 ± 0.38	ND
4	**7.81 ± 0.52**	**5.99 ± 0.23**	**7.41 ± 0.32**	**6.18 ± 1.15**	**15.28 ± 1.26**	**81.37 ± 0.10**
5	29.35 ± 0.52	17.38 ± 1.05	28.31 ± 1.52	28.37 ± 0.16	52.75 ± 0.81	ND
L	55.09 ± 0.81	45.35 ± 0.32	60.57 ± 0.27	19.38 ± 1.07	88.27 ± 0.28	ND
Cisplatin	5.78 ± 0.12	3.25 ± 0.23	4.63 ± 0.13	4.90 ± 0.31	10.52 ± 0.40	ND

Values are expressed as mean ± SEM. Cytotoxicity as IC_{50} for each cell line is the concentration of compound which is reduced by 50% the optical density of treated cell with respect to untreated cell using the MTT assay

ND not determined

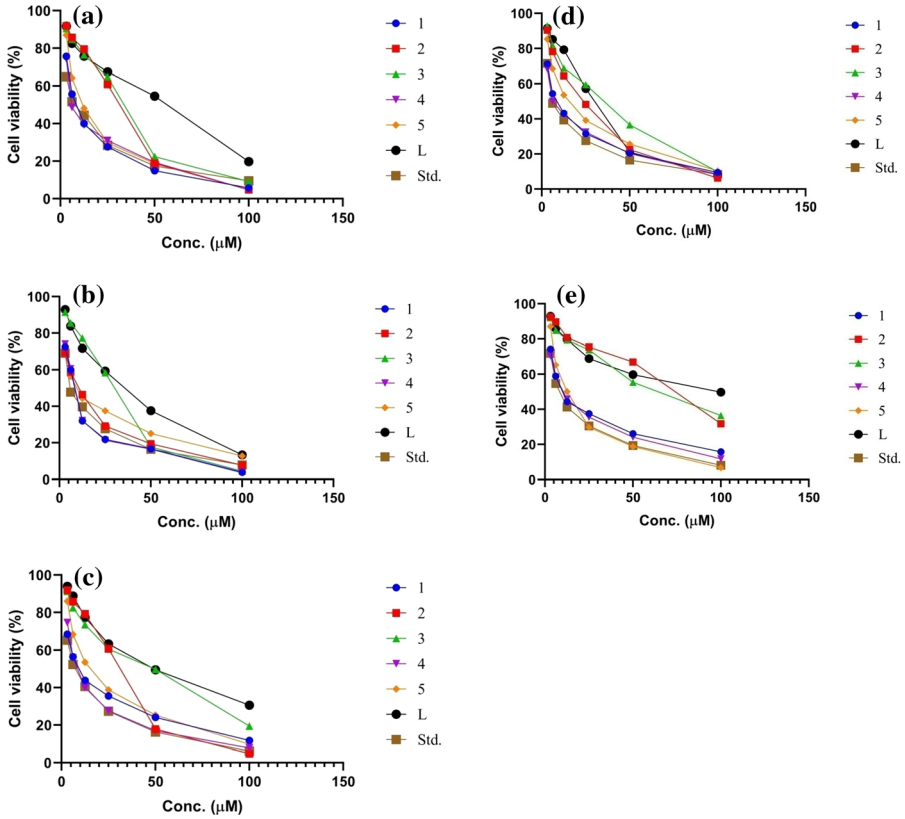

Fig. 9 Survival curves of cell lines: **a** IMR-32, **b** HeLa, **c** MCF-7 **d** A549 and **e** HepG-2

Synthesis of 4-(((2-aminopyridin-3-yl)methylene)amino)benzoic acid (L)

A mixture of 2-aminonicotinaldehyde (1.22 g, 10 mmol) and 4-aminobenzoic acid (1.37 g, 10 mmol) in methanol was stirred for 1 h, to obtain the yellow color precipitate. The product was collected by filtration, washed with methanol and dried in a desiccator over calcium chloride. Yield: 95%. Yellow color solid. M.p.: 270–272 °C. Anal. Calcd. for $C_{13}H_{11}N_3O_2$ (%): C, 64.72; H, 4.60; N, 17.42. Found: C, 64.65; H, 4.56; N, 17.48. FT-IR (KBr): υ, cm^{-1} 3420 (N − H), 1629 (C=N), 1567 $(C=N)_{py}$, 1701 $(C=O)_{carbaxilic\ acid}$. ^{1}H NMR (400 MHz, DMSO) δ: 12.93 (s, 1H, OH), 8.72 (s, 1H, CH=N), 8.14 (d, *J* = 6.0 Hz, 1H, aromatic-H), 8.00–7.87 (m, 5H, aromatic-H), 7.38 (s, 2H, NH_2), 6.72–6.69 (m, 1H, aromatic-H). ^{13}C NMR (100 MHz, DMSO) δ: 167.49, 163.88, 158.44, 155.10, 152.18, 143.40, 131.11, 128.37, 121.77, 112.46, 112.34.

Synthesis of metal complexes (1–5)

An appropriate amount of methanolic solution of ligand (2 mmol, 0.482 g) and methanolic solution containing the chlorides of the Co(II), Ni(II), Cu(II), Zn(II) and Pd(II) (1 mmol) were mixed with constant stirring for 4 h under reflux, and then the precipitate formed collected by filtration, washed with methanol and dried in a desiccator over calcium chloride.

Table 13 Binding energies of ligand and its metal complexes (**1–5**) against protein receptors **HER 2** and **EGFR**

HER2 (PDB ID: 3POZ)					EGFR (PDB ID: 4HJO)			
Compound	Binding energy (kcal/mol)	No. of hydrogen bonds	Amino acid residues involved in the hydrogen bonding	Hydrogen bond length (Å)	Binding energy (kcal/mol)	No. of hydrogen bonds	Amino acid residues involved in the hydrogen bonding	Hydrogen bond length (Å)
1	**− 7.31**	**4**	**SER720, GLY724, ALA722, LYS875**	**1.80, 2.28, 2.90, 3.03**	**− 6.46**	**8**	**ARG817, ASP813, ASP831, LYS721, CYS773, GLY697**	**1.87, 2.08, 2.14, 2.87, 3.04, 3.14, 3.16, 3.28**
2	− 7.08	4	MET793, ASP800, ASP855, CYS797	2.00, 2.37, 2.75, 3.09	− 6.02	4	ALA698, PHE699, GLY700, SER696	1.67, 2.44, 2.51, 2.35
3	− 7.20	5	CYS797, ARG841, ASP800, ALA722, ASP855	2.08, 2.26, 2.88, 2.96, 3.02	− 6.10	6	ARG779, LYS851, SER696, GLY695, SER696	1.79, 1.85, 1.91, 2.51, 2.89, 3.53
4	**− 8.02**	**5**	**LYS875, ASP837, PRO877, ALA722, GLY719**	**1.69, 1.85, 3.56, 3.69, 3.77**	**− 7.35**	**8**	**ARG779, GLY695, LYS851, LYS889, SER696**	**1.61, 1.92, 1.93, 1.95, 2.97, 2.98, 3.37, 3.57**
5	− 6.37	4	CYS797, ASP800, MET793	2.07, 2.09, 2.17, 2.31	− 6.42	3	ASP831, GLN767, PHE832	1.73, 2.77, 3.38
L	− 6.62	3	MET793, ASP855, GLN791	1.80, 1.84, 2.09	− 5.56	5	LYS851, LYS721, ASN818	2.00, 2.65, 3.06, 1.95
Canertinib	− 7.73	2	ASN842, THR854	1.89, 3.36	–	–	–	–
Afatinib	− 6.37	3	ASP800, ARG841, LYS745	2.71, 2.86, 2.56	–	–	–	–
Lapatinib	–	–	–	–	− 5.94	3	CYS773, LYS721	3.08, 2.29, 2.95
Gefitinib	–	–	–	–	− 6.60	6	ASP813, LYS721, ASP831, ARG817	3.03, 2.98, 2.85, 2.97, 1.82, 2.23

[Co(II)(L)$_2$Cl$_2$] (1)

$CoCl_2$ $6H_2O$ (0.237 g, 1 mmol) was used. Brown, Yield: 71%. M.p.: 350–352 °C. Anal. Calcd. for $C_{26}H_{22}Cl_2CoN_6O_4$ (%): C, 50.93; H, 3.65; N, 13.66; Co, 9.62. Found: C, 50.93; H, 3.65; N, 13.66; Co, 9.69. $\wedge^m$ = 12. UV–Vis (DMF): λ_{max}, nm (cm^{-1}) 1111 (9000), 540 (18,500), 490 (20,400). FT-IR (KBr): υ, cm^{-1} 3371 (N–H), 1604 (C=N), 1564 $(C=N)_{py}$, 1699 $(C=O)_{carbaxilic\ acid}$. μ = 4.95 BM.

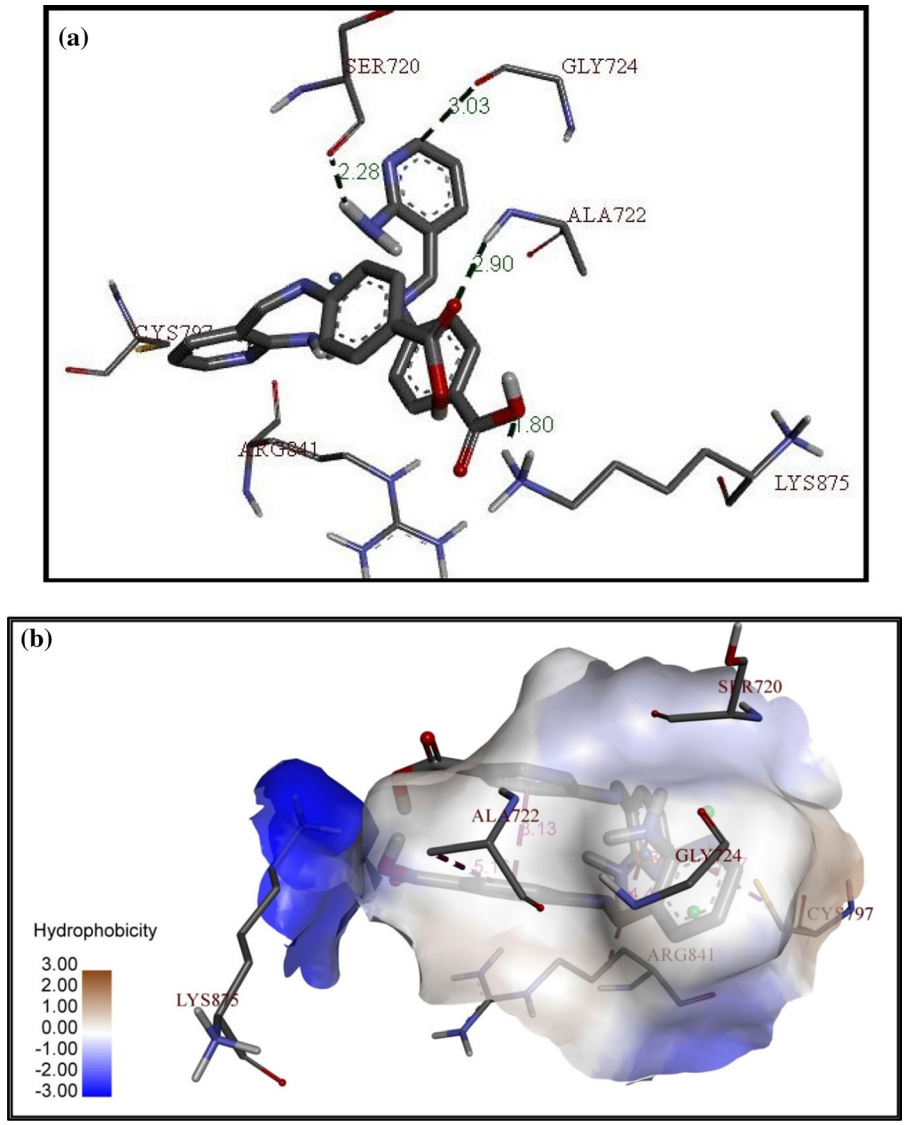

Fig. 10 The best docking pose of complex **1** with HER2. **a** Hydrogen bond interactions, **b** hydrophobic interactions

[Ni(II)(L)$_2$Cl$_2$] (2)

$NiCl_2$ $6H_2O$ (0.237 g, 1 mmol) was used. Yield: 79%. Light green. M.p.: 310–312 °C. Anal. Calcd. for $C_{26}H_{22}Cl_2N_6NiO_4$ (%): C, 51.02; H, 3.62; N, 13.73; Ni, 9.59. Found: C, 50.97; H, 3.58; N, 13.67; Ni, 9.52. $\wedge^m$ = 16. UV–Vis (DMF): λ_{max}, nm (cm^{-1}) 1020 (9800), 628 (15,900), 387 (25,800). FT-IR (KBr): υ, cm^{-1} 3389 (N–H), 1663 (C=N), 1569 $(C=N)_{py}$, 1704 (C=O). μ = 3.22 BM.

[Cu(II)(L)$_2$Cl$_2$] (3)

$CuCl_2$ (0.134 g, 1 mmol) was used. Yield: 84%. green. M.p.: 328–330 °C. Anal. Calcd. for $C_{26}H_{22}Cl_2CuN_6O_4$ (%): C, 50.62; H, 3.59; N, 13.62; Cu, 10.30.

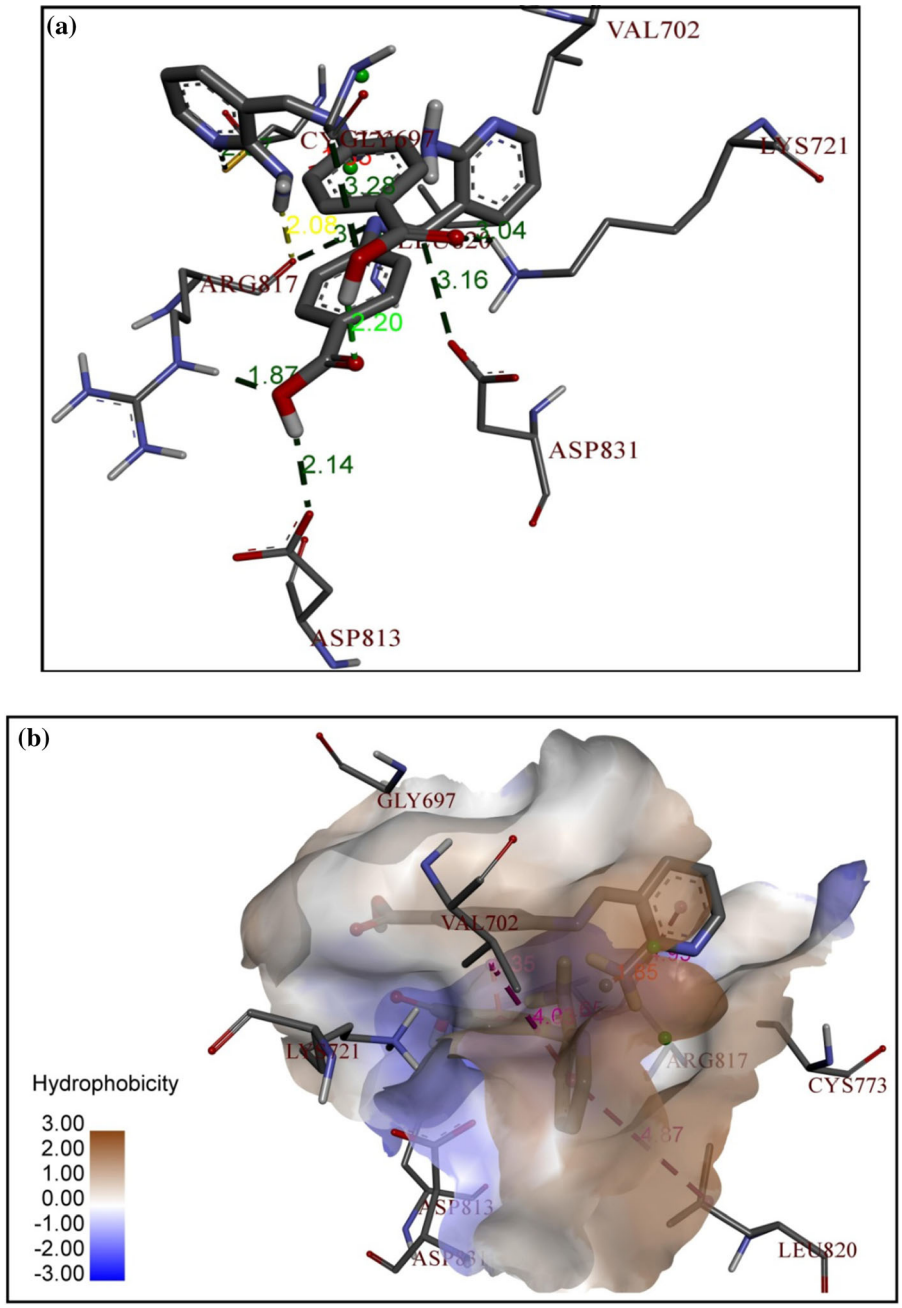

Fig. 11 The best docking pose of complex **1** with EGFR. **a** Hydrogen bond interactions, **b** hydrophobic interactions

Found: C, 50.58; H, 3.55; N, 13.59; Cu, 10.25. $\wedge^{m}$ = 19. UV–Vis (DMF): λ_{max}, nm (cm^{-1}) 544 (18,351), 723 (13,825). FT-IR (KBr): υ, cm^{-1} 3390 (N–H), 1592 (C=N), 1562 $(C=N)_{py}$, 1703 (C=O). μ = 1.83 BM. EPR 'g' values 2.22, 2.05.

[Zn(II)(L)$_2$Cl$_2$] (4)

$ZnCl_2$ (0.136 g, 1 mmol) was used. Light Yellow. Yield: 75%. M.p.: 378–380 °C. Anal. Calcd. for $C_{26}H_{22}Cl_2N_6O_4Zn$ (%): C, 50.47; H, 3.58; N, 13.58;

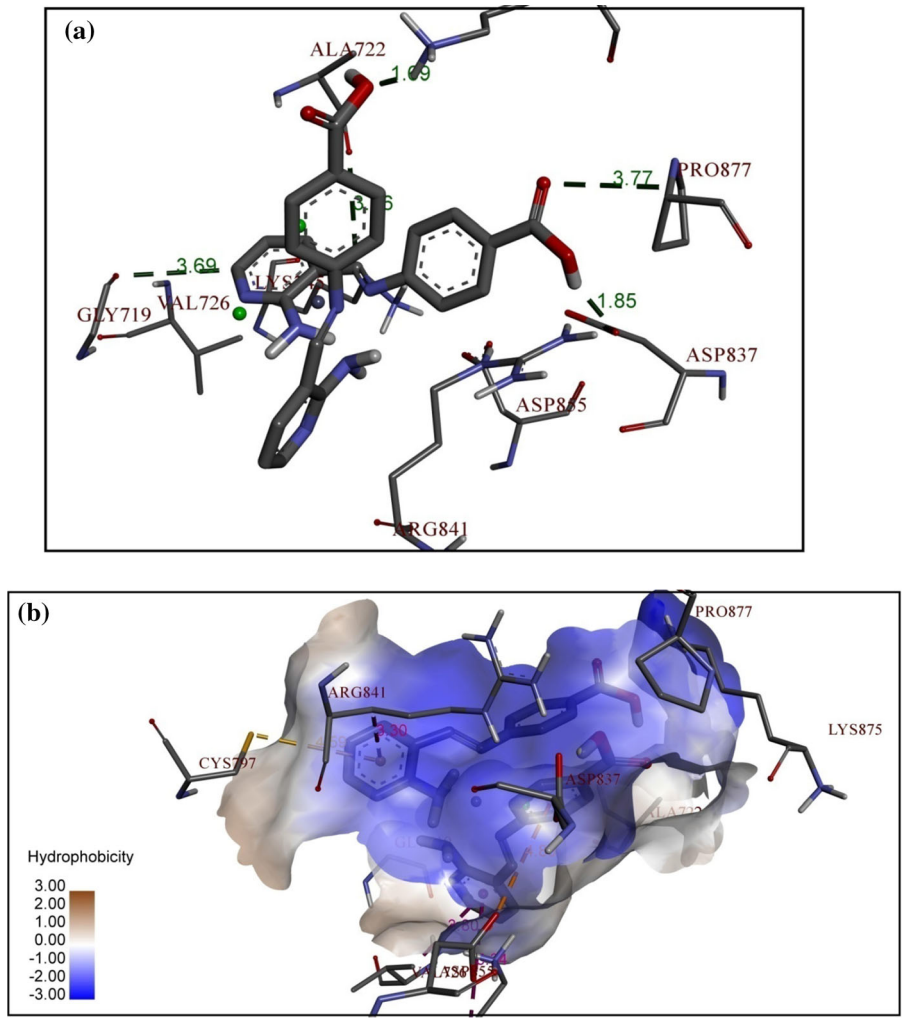

Fig. 12 The best docking pose of complex **4** with HER2. **a** Hydrogen bond interactions, **b** hydrophobic interactions

Zn, 10.57. Found: C, 50.41; H, 3.55; N, 13.54; Zn, 10.50. $\wedge^{m}$ = 15. FT-IR (KBr): υ, cm^{-1} 3384 (N–H), 1592 (C=N), 1571 $(C=N)_{py}$, 1697(C=O). ^{1}H NMR (400 MHz, DMSO): δ: 12.07 (s, 1H, OH), 8.74 (s, 1H, CH=N), 8.13–7.91 (m, 6H, aromatic-H), 7.33 (s, 2H, NH_2), 6.72 (s, 1H, aromatic-H). ^{13}C NMR (100 MHz, DMSO) δ: 166.98, 163.78, 157.30 154.88, 152.08, 142.96, 131.01, 129.01, 121.67, 112.42, 112.31.

[Pd(II)(L)Cl_2] (5)

Pd(II) chloride (0.177 g, 1 mmol) was used. Yield: 88%. Orange. M.p.: 336–338 °C. Anal. Calcd. for $C_{13}H_{11}Cl_2N_3O_2Pd$ (%): C, 37.30; H, 2.65; N, 10.04; Pd, 25.42. Found: C, 37.37; H, 2.59; N, 10.09; Pd, 25.31. $\wedge^{m}$ = 11. UV–Vis (DMF): λ_{max}, nm (cm^{-1}) 534 (18,700), 465 (21,500), 402 (24,855), 357 (28,000). FT-IR (KBr): υ, cm^{-1} 3401 (N–H), 1608(C=N), 1570 $(C=N)_{py}$, 1705 (C=O). ^{1}H NMR (400 MHz, DMSO) δ: 12.82 (s, 1H, OH), 8.61 (s, 1H, CH=N), 8.03 (d, *J* = 6.0 Hz, 1H, aromatic-H),

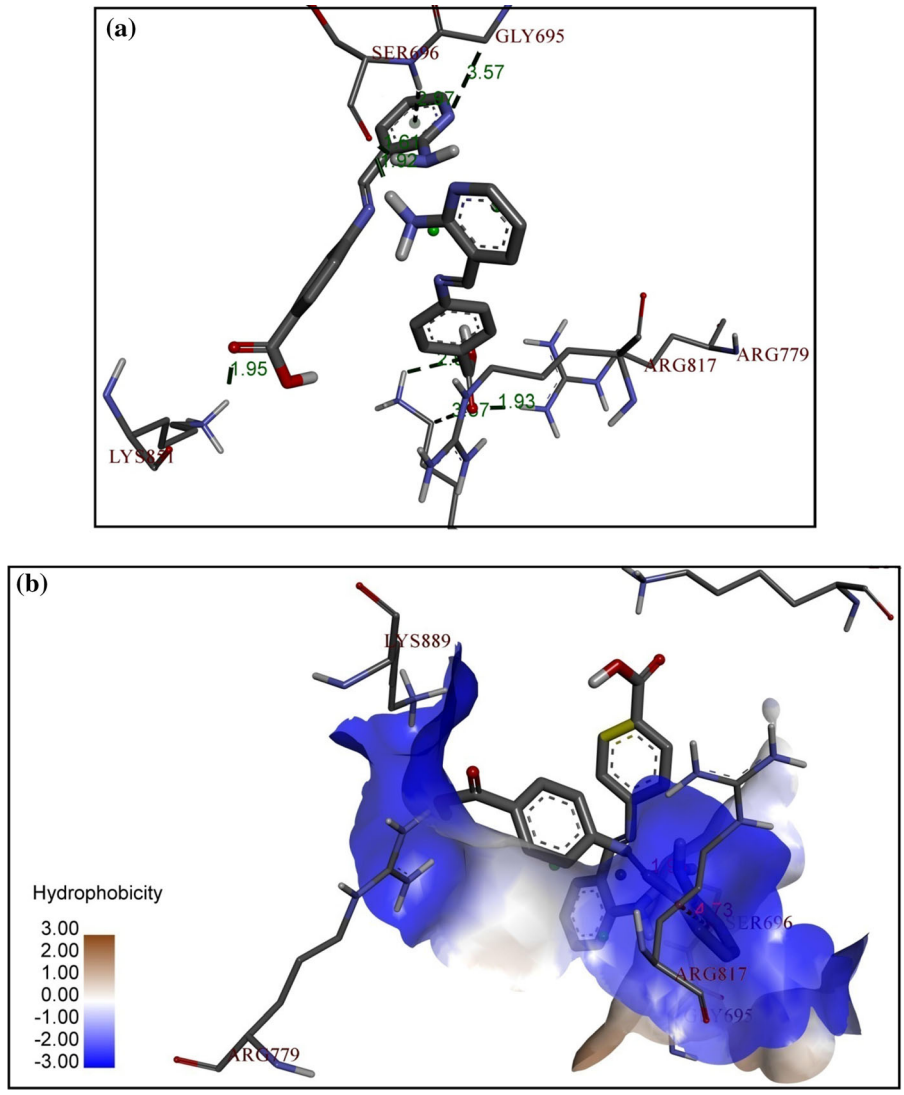

Fig. 13 The best docking pose of complex **4** with EGFR. **a** Hydrogen bond interactions, **b** hydrophobic interactions

7.89–7.77 (m, 5H, aromatic-H), 7.28 (s, 2H, NH_2), 6.62–6.59 (m, 1H, aromatic-H). ^{13}C NMR (100 MHz, DMSO) δ: 167.39, 163.79, 158.44, 155.00, 152.09, 143.30, 131.01, 128.27, 121.68, 112.36, 112.25.

Biological evaluations

The methods used for antibacterial, antifungal, radical scavenging, and in vitro anti-proliferative activity studies were explained in the supplementary information file.

Acknowledgements Ramaiah Konakanchi, thanks the Department of Chemistry NIT Warangal and Malla Reddy Engineering College for Women (Autonomous Institution), Hyderabad, India, for support and encouragement during this research work.

References

Abdel Aziz AA, El-Sayed ISA, Khalil MMH (2017a) Some divalent metal(II) complexes of novel potentially tetradentate schiff base N,N′-bis(2-carboxyphenylimine)-2,5-thiophenedicarboxaldhyde: synthesis, spectroscopic

characterization and bioactivities. Appl Organomet Chem 31:e3730

Abdel Aziz AA, Elantabli FM, Moustafa H et al (2017b) Spectroscopic, DNA binding ability, biological activity, DFT calculations and non linear optical properties (NLO) of novel Co(II), Cu(II), Zn(II), Cd(II) and Hg(II) complexes with ONS schiff base. J Mol Struct 1141:563–576

Abdel-Rahman LH, Abu-Dief AM, Hamdan SK et al (2015) Nano structure iron (II) and copper (II) schiff base complexes of a NNO-tridentate ligand as new antibiotic agents: spectral, thermal behaviors and DNA binding ability. Int J Nano Chem 1:65–77

Abdel-Rahman LH, Abu-Dief AM, Newair EF, Hamdan SK (2016) Some new nano-sized Cr(III), Fe(II), Co(II), and Ni(II) complexes incorporating 2-((*E*)-(pyridine-2-ylimino)methyl)napthalen-1-ol ligand: structural characterization, electrochemical, antioxidant, antimicrobial, antiviral assessment and DNA interaction. J Photochem Photobiol B 160:18–31

Abu Al-Nasr AK, Ramadan RM (2013) Spectroscopic studies and biological activity of some transition metal complexes of unusual schiff base. Spectrochim Acta A 105:14–19

Arivazhagan M, Jeyavijayan S (2011) Vibrational spectroscopic, first-order hyperpolarizability and HOMO, LUMO studies of 1,2-dichloro-4-nitrobenzene based on Hartree-Fock and DFT calculations. Spectrochim Acta A 79:376–383

Arun T, Packianathan S, Malarvizhi M et al (2015) Bio-relevant complexes of novel N_2O_2 type heterocyclic ligand: synthesis, structural elucidation, biological evaluation and docking studies. J Photochem Photobiol B 149:93–102

Becke AD (1993) Density-functional thermo chemistry. III. The role of exact exchange. J Chem Phys 98:5648–5652

Bergner A, Dolg M, Kuechle W et al (1993) *Ab initio* energy-adjusted pseudo potentials for elements of groups 13–17. Mol Phys 80:1431–1441

Breneman CM, Wiberg KB (1990) Determining atom-centered monopoles from molecular electrostatic potentials: the need for high sampling density in formamide conformational analysis. J Comput Chem 11:361–373

Buckingham AD (1967) Permanent and induced molecular moments and long-range inter molecular forces. Adv Chem Phys 12:107–142

Burns GR (1968) Metal complexes of thiocarbohydrazide. Inorg Chem 7:277–283

Buza N, Roque DM, Santin AD (2014) HER2/neu in endometrial cancer: a promising therapeutic target with diagnostic challenges. Arch Pathol Lab Med 138:343–350

Chandra S (2004) Spectroscopic, redox and biological activities of transition metal complexes with O N, S donor macrocyclic ligand derived from semicarbazide and thiodiglycolic acid. Spectrochim Acta A 60:2153–2162

Choi CH, Kertez M (1997) Conformational information from vibrational spectra of styrene, *trans*-stilbene, and *cis*-stilbene. J Phys Chem A 101:3823–3831

Cotton FA, Wilkinson G, Murillo CA, Bochmann M (1999) Advanced Inorganic Chemistry, 6th edn. Wiley, New York

Davis AM, Teague SJ (1999) Hydrogen bonding, hydrophobic interactions and failure of the rigid receptor hypothesis. Angew Chem Int Ed 38:736–749

Dev J, Batra N, Malhotra R (2012) Ligational behavior of Schiff bases towards transition metal ion and metallation effect on their antibacterial activity. Spectrochim Acta A 97:397–405

Devi J, Yadav M, Kumar A (2018a) Synthesis, characterization, biological activity, and QSAR studies of transition metal complexes derived from piperonylamine schiff bases. Chem Pap 72:2479–2502

Devi J, Yadav M, Kumar D, Naik LS, Jindal DK (2018b) Some divalent metal(II) complexes of salicylaldehyde derived schiff bases: synthesis, spectroscopic characterization, antimicrobial and in vitro anticancer studies. Appl Organomet Chem 33:e4693

Dolg M, Stoll H, Preuss H, Pitzer RM (1993) Relativistic and correlation effects for element 105 (hahnium, Ha): a comparative study of M and MO (M = Nb, Ta, Ha) using energy-adjusted *ab initio* pseudopotentials. J Phys Chem 97:5852–5859

Ebrahimi HP, Hadi JS, Abdulnabi ZA, Bolandnazar Z (2014) Spectroscopic, thermal analysis and DFT computational studies of salen-type schiff base complexes. Spectrochim Acta A 117:485–492

El-Boraey HA, El-Salamony MA (2019) Transition metal complexes with polydentate ligand: synthesis, characterization, 3D molecular modelling, anticancer, antioxidant and antibacterial evaluation. J Inorg Organomet Polym 29:684–700

Firdaus F, Fatma K, Azam M, Khan SN, Khan AU, Shakir MN (2009) Metal ion controlled synthesis of 16- and 18-membered binuclear octaaza macrocyclic complexes with Co(II), Ni(Il), Cu(II) and Zn(II): a comparative spectroscopic approach to DNA binding to Cu(II) complexes. Spectrochim Acta A 72:591–596

Foloppe N, MacKerell AD (2000) All-atom empirical force field for nucleic acids: I. parameter optimization based on small molecule and condensed phase macromolecular target data. J Comput Chem 21:86–104

Frisch MJ, Trucks GW, Schlegel HB, Scuseria GE, Robb MA, Cheeseman JR, Scalmani G, Barone V, Mennucci B, Petersson GA, Nakatsuji H, Caricato M, Li X, Hratchian HP, Izmaylov AF, Bloino J, Zheng G, Sonnenberg JL, Hada M, Ehara M, Toyota K, Fukuda R, Hasegawa J. Ishida M, Nakajima T, Honda Y, Kitao O, Nakai H, Vreven T, Montgomery Jr JA, Peralta JE, Ogliaro F, Bearpark M, Heyd JJ, Brothers E, Kudin KN, Staroverov VN, Kobayashi R, Normand J, Raghavachar K, Rendell A, Burant JC, Iyengar SS, Tomasi J, Coss M, Rega N, Millam JM, Klene M, Knox JE, Cross JB, Bakken V, Adamo C, Jaramillo J, Gomperts R, Stratmann RE, Yazyev O, Austin AJ, Cammi R, Pomelli C, Ochterski JW, Martin RL, Morokuma K, Zakrzewski VG, Voth GA, Salvador P, Dannenberg JJ, Dapprich S, Daniels AD, Foresman JB, Ortiz JV, Cioslowski J, Fox DJ (2010) Gaussian 09, Revision B.01, Gaussian, Inc., Wallingford CT

Fukui K (1982) Role of frontier orbitals in chemical reactions. Science 218:747–754

Gajendragad MR, Aggarwala UC (1975) Complexing behaviour of 1,3,4-thiadiazole-2-thiol-5-amino-I. Complexes of Fe(II), Co(II), Ru(III), Ru(II), Rh(III), Pd(IV), Ir(III) and Pt(IV). J Inorg Nucl Chem 37:2429–2434

Ganesan K, Ponya Utthra P, Dharmasivam M, Natarajan R (2019) Exploring the DNA interactions, FGF growth receptor interaction and biological screening of metal(II) complexes of NNN donor ligand derived from 2(aminomethyl)benzimidazole. Int J Biol Macromol 126:1303–1317

Gece G (2008) The use of quantum chemical methods in corrosion inhibitor studies. Corros Sci 50:2981–2992

Global, regional, and national life expectancy, all-cause mortality, and cause-specific mortality for 249 causes of death, 1980–2015: a systematic analysis for the Global Burden of Disease Study 2015, 2016. Lancet 388:1459–1544

Goggin PL, Goodfellow RJ, Reed FJS (1972) Trimethylamine complexes of platinum(II) and palladium(II) and their vibrational and proton nuclear magnetic resonance spectra. J Chem Soc Dalton Trans 12:1298–1303

Gul MZ, Ahmad F, Kondapi AK et al (2013) Antioxidant and antiproliferative activities of abrus precatorius leaf extracts-an in vitro study. Complem Altern Med 13:53–65

Hathaway BJ, Billing DE (1970) The electronic properties and stereochemistry of mono-nuclear complexes of the copper(II) ion. Coord Chem Rev 5:143–207

Hinchliffe F, Munn RW (1985) Molecular electromagnetism. Wiley, New York

Jost C, Schilling J, Tamaskovic R, Schwill M, Honegger A, Pluckthun A (2013) Structural basis for eliciting a cytotoxic effect in HER2-overexpressing cancer cells via binding to the extracellular domain of HER2. Structure 21:1979–1991

Jyothi S, Sreedhar K, Nagaraju D et al (2015) Synthesis and spectral investigation of Co(II), Ni(II), Cu(II) and Zn(II) complexes with novel N4 ligands. Can Chem Trans 3:368–380

Kaupp M, Schleyer PVR, Stoll H et al (1991) Pseudopotential approaches to Ca Sr and Ba hydrides why are some alkaline earth MX2 compounds bent. J Chem Phys 94:1360

Kavitha P, Laxma Reddy K (2012) Synthesis, spectral characterisation, morphology, biological activity and DNA cleavage studies of metal complexes with chromone Schiff base. Arabian J Chem 9:596–605

Kavitha P, Saritha M, Laxma Reddy K (2013) Synthesis, structural characterization, fluorescence, antimicrobial, antioxidant and DNA cleavage studies of Cu(II) complexes of formyl chromone schiff bases. Spectrochim Acta A 102:159–168

Kelland L (2007) The resurgence of platinum-based cancer chemotherapy. Nat Rev Cancer 7:573–584

Khedr M, Marwani HM (2012) Synthesis, spectral, thermal analyses and molecular modeling of bioactive Cu(II)-complexes with 1,3,4-thiadiazole schiff base derivatives. their catalytic effect on the cathodic reduction of oxygen. Int J Electrochem Sci 7:10074–10093

Kivelson D, Neiman R (1961) ESR studies on the bonding in copper complexes. J Chem Phys 35:149–155

Kleinman DA (1962) Nonlinear dielectric polarization in optical media. Phys Rev 126:1977–1979

Kneubuhl FK (1960) Line shapes of electron paramagnetic resonance signals produced by powders, glasses, and viscous liquids. J Chem Phys 33:1074–1078

Konakanchi R, Haribabu J, Prashanth J et al (2018a) Synthesis, structural, biological evaluation, molecular docking and DFT studies of Co(II), Ni(II), Cu(II), Zn(II), Cd(II) and Hg(II) complexes bearing heterocyclic thiosemicarbazone ligand. Appl Organomet Chem 32:e4415

Konakanchi R, Mallela R, Guda R, Kotha LR (2018b) Synthesis, characterization, biological screening and molecular docking studies of 2-aminonicotinaldehyde (ANA) and its metal complexes. Res Chem Intermed 44:27–53

Koopmans TA (1933) Ordering of wave functions and eigen energies of the individual electrons of an atom. Physica 1:104–113

Kosar D, Albayrak C (2011) Spectroscopic investigations and quantum chemical computational study of (*E*)-4-methoxy-2-[(p-tolylimino)methyl]phenol. Spectrochim Acta A 78:160–167

Lee C, Yang W, Parr RG (1988) Development of the Colic-Salvetti correlation energy formula into a functional of the electron density. Phys Rev B 37:785–789

Lewis DFV, Ioannides C, Parke DV (1994) Interaction of a series of nitriles with the alcohol-inducible isoform of P450: computer analysis of structure-activity relationships. Xenobiotica 24:401–408

Lynch TJ, Bell DW, Sordella R et al (2004) Activating mutations in the epidermal growth factor receptor under lying responsiveness of non-small-cell lung cancer to gefitinib. N Engl J Med 350:2129–2139

Mahmoud WH, Deghad RG, El Desssouky MMI, Mohamed GG (2018) Transition metal complexes of nano bidentate organometallic Schiff base: preparation, structure characterization, biological activity, DFT and molecular docking studies. Appl Organomet Chem 33:e4556

Mallela R, Konakanchi R, Guda R et al (2018) Zn(II), Cd(II) and Hg(II) metal complexes of 2-aminonicotinaldehyde: synthesis, crystal structure, biological evaluation and molecular docking study. Inorganica Chim Acta 469:66–75

Mesbah M, Douadia T, Sahli F et al (2018) Synthesis, characterization, spectroscopic studies and antimicrobial activity of three new schiff bases derived from heterocyclic moiety. J Mol Struct 1151:41–48

Meyers F, Marder SR, Pierce BM et al (1994) Electric field modulated nonlinear optical properties of donor-acceptor polyenes: sum-over-states investigation of the relationship between molecular polarizabilities and bond length alternation. J Am Ceram Soc 116:10703–10714

Miri R, Razzaghi-asl N, Mohammadi MK (2013) QM study and conformational analysis of an isatin schiff base as a potential cytotoxic agent. J Mol Model 19:727–735

Mohamed GG, El-Gamel NEA, Nour El-Dien FA (2001) Preparation, chemical characterization, and electronic spectra of 6-(2-pyridylzo)-3-actamidophenol and its metal complexes. Synth React Inorg Met Org Chem 31:347–358

Mohammadtabar F, Shafaatian B, Soleymanpour A, Rezvani SA et al (2016) Synthesis, spectral characterization, X-ray crystal structure, electrochemical studies, and DNA interactions of a Schiff base pro-ligand and its homobimetallic complexes containing the cysteamine moiety. Transition Met Chem 41:475–484

Mohanraj M, Ayyannan G, Raja G, Jayabalakrishnan C (2016) Synthesis, spectral characterization, DNA interaction, radical scavenging and cytotoxicity studies of ruthenium(II) hydrazone complexes. J Photochem Photobiol B 158:164–173

Mosmann T (1983) Rapid colorimetric assay for cellular growth and survival: application to proliferation and cytotoxicity assays. J Immunol Meth 65:5–63

Mumtaz A, Mahmud T, Elsegood MR, Weaver GW (2016) Synthesis and characterization of new schiff base transition metal complexes derived from drug together with biological potential study. J Nucl Med Radiat Ther 7:310–318

Muralisankar M, Bhuvanesh NSP, Sreekanth A (2016) Synthesis, X ray crystal structure, DNA/protein binding and DNA cleavage studies of novel copper(II) complexes of *N*-substituted isatin thiosemicarbazone ligands. New J Chem 40:2661–2679

Nigam S, Patel MM, Ray A (2000) Normal coordinate analyses and CNDO/II calculations of isonitrosopropiophenone (propiophenone oxime), and its semicarbazone and thiosemicarbazone derivatives: synthesis and characterization of their metal complexes. J Phys Chem Sol 61:1389–1398

Omar MM, Mohamed GG (2005) Potentiometric, spectroscopic and thermal studies on the metal chelates of 1-(2-thiazolylazo)-2-naphthalenol. Spectrochim Acta A 61:929–936

Parr RJ, Szentpa'ly LV, Liu S (1999) Electrophilicity index. J Am Chem Soc 121:1922–1924

Patil SA, Kulkarni VH (1984) Spectral and magnetic studies of tin(IV) complexes with nickel(II) thiocarbohydrazones. Polyhedron 3:21–24

Prasad PN, Williams DJ (1991) Introduction to nonlinear optical effects in molecules and polymers. Wiley, New York

Ramadan AEM (2012) Macrocyclic nickel(II) complexes: synthesis, characterization, superoxide scavenging activity and DNA-binding. J Mol Struct 1015:56–66

Ramadan RM, Abu Al-Nasr AK, Noureldeen AFH (2014) Synthesis, spectroscopic studies, antimicrobial activities and antitumor of a new monodentate V-shaped Schiff base and its transition metal complexes. Spectrochim Acta A 132:417–422

Ramadan RM, Elsheemy WM, Hassan NS, Abdel Aziz AA (2018) Synthesis, spectroscopic characterization, thermal behaviour, in vitro antimicrobial and anticancer activities of novel ruthenium tricarbonyl complexes containing monodentate V-shaped Schiff bases. Appl Organomet Chem 32:e4180

Raman N, Ravichandran S, Thangaraja C (2004) Copper(II), cobalt(II), nickel(II) and zinc(II) complexes of Schiff base derived from benzil-2,4-dinitrophenylhydrazone with aniline. J Chem Sci 116(4):215–219

Rohini G, Haribabu J, Aneesrahman KN et al (2018a) Half-sandwich Ru(II)(η^6-p-cymene) complexes bearing *N*-dibenzosuberenyl appended thiourea for catalytic transfer hydrogenation and in vitro anticancer activity. Polyhedron 152:147–154

Rohini G, Ramaiah K, Aneesrahman KN, Sreekanth A (2018b) Biological evaluation, DNA/protein-binding aptitude of novel dibenzosuberene appended palladium (II)-thiourea complexes. Appl Organomet Chem 32:e4567

Sabastiyan A, Venkappayya DJ (1990) Spectral and microbiological study of quinoxalinium dichromate. Indian Chem Soc 67:584–590

Saif M, Mashaly MM, Eid MF et al (2011) Synthesis and thermal studies of tetraaza macrocylic ligand and its transition metal complexes, DNA binding affinity of copper complex. Spectrochim Acta A 79:1849–1855

Saif M, Mashaly MM, Eid MF, Fouad R (2012) Synthesis, characterization and thermal studies of binary and/or mixed ligand complexes of Cd(II), Cu(II), Ni(II) and Co(III) based on 2-(hydroxybenzylidene) thiosemicarbazone: DNA binding affinity of binary Cu(II) complex. Spectrochim Acta A 92:347–356

Saleh AA (2005) Synthesis and spectroscopic studies of novel mononuclear complexes of cyclic and acyclic Schiff-base derivatives of tridentate and tetradentate coordination with some bivalent transition metal ions. J Coord Chem 58:255–270

Santin AD, Bellone S, Roman J, McKenney JK (2008) Trastuzumab treatment in patients with advanced or recurrent endometrial carcinoma overexpressing HER2/neu. Int J Gynecol Obstet 102:128–131

Sathyadevi P, Krishnamoorthy P, Jayanthi E (2012) Studies on the effect of metal ions of hydrazone complexes on interaction with nucleic acids, bovine serum albumin and antioxidant properties. Inorganica Chim Acta 384:83–96

Schroeder RL, Stevens CL, Sridhar J (2014) Small molecule tyrosine kinase inhibitors of ErbB2/HER2/Neuin the treatment of aggressive breast cancer. Molecules 19:15196–15212

Sebastian J, Richards RG, Walker MP et al (1998) Activation and function of the epidermal growth factor receptor and erbB-2 during mammary gland morphogenesis. Cell Growth Differ 9:777–785

Shukla D, Gupta LK, Chandra S (2008) Spectroscopic studies on chromium(III), manganese(II), cobalt(II), nickel(II) and copper(II) complexes with hexadentate nitrogen-sulfur donor [N_2S_4] macrocyclic ligand. Spectrochim Acta A 71:746–750

Sinha L, Prasad O, Naryan V, Shukla SR (2011) Raman, FT-IR spectroscopic analysis and first-order hyperpolarisability of 3-benzoyl-5-chlorouracil by first principles. J Mol Simul 37:153–163

Srividya S, Jebiti H, Naveen Kumar K et al (2019) Synthesis and anticancer activity of ruthinium arene complexes-high activity against IMR-32 cancer cell line. ACS omega 4:6245–6256

Thirunavukkarasu T, Sparkes HA, Natarajan K, Gnanasoundari VG (2018) Synthesis, characterization and biological studies of a novel Cu(II) schiff base complex. Inorganica Chim Acta 473:255–262

Walker F, Abramowitz L, Benabderrahmane D et al (2009) Growth factor receptor expression in anal squamous lesions: modifications associated with oncogenic human papillomavirus and human immune deficiency virus. Hum Pathol 40:1517–1527

Wernyj RP, Morin PJ (2004) Molecular mechanisms of platinum resistance: still searching for the Achilles' heel, drug resist. Update 7:227–232